Type II kinase inhibitors targeting the Cys-gatekeeper display orthogonality with wild type and Ala/Gly-gatekeeper kinases

Cory A. Ocasio*[a,f+], Alexander A. Warkentin[b+], Patrick J. McIntyre[c], Krister J. Barkovich[b], Clare Vesely[a], John Spencer[d], Kevan M. Shokat[b] and Richard Bayliss[e]

[a] Dr. Cory A. Ocasio*[+], Dr. Clare Vesely
Genome Damage and Stability Centre, School of Life Sciences, University of Sussex, Falmer, Brighton, BN1 9RQ (UK)
[b] Dr. Alexander A. Warkentin[+], Krister J. Barkovich, MD, Professor Kevan M. Shokat
Howard Hughes Medical Institute and Department of Cellular and Molecular Pharmacology, University of California, San Francisco, 600 16th Street, San Francisco, CA, 94158-2280 (US)
[c] Dr. Patrick J. McIntyre
Department of Molecular and Cell Biology, Henry Wellcome Building, University of Leicester, Leicester, LE1 9HN, (UK)
[d] Professor John Spencer
Department of Chemistry, School of Life Sciences, University of Sussex, Falmer, Brighton, BN1 9QJ (UK)
[e] Professor Richard Bayliss
School of Molecular and Cellular Biology, Faculty of Biological Sciences, University of Leeds, Leeds, LS2 9JT (UK)
[f] Current Address: The Francis Crick Institute, London, NW1 1AT (UK)
[+] Denotes joint first authors
[*] Correspondence: Cory A. Ocasio; tony.ocasio@crick.ac.uk

Supporting information for this article is given via a link at the end of the document

Abstract. Analog-sensitive (AS) kinases contain large to small mutations in the gatekeeper position rendering them susceptible to inhibition with bulky analogs of pyrazolopyrimidine-based Src kinase inhibitors (*e.g.* PP1). This 'bump-hole' method has been utilized for at least 85 of ~520 kinases, but many kinases are intolerant to this approach. To expand the scope of AS-kinase technology, we designed type II kinase inhibitors, **ASDO2/6** (**A**nalog-**S**ensitive '**D**FG-**O**ut' kinase inhibitors-**2**/**6**), that target the 'DFG-out' conformation of cysteine (Cys)-gatekeeper kinases with submicromolar potency. We validated this system *in vitro* against Greatwall kinase (GWL), Aurora-A kinase and Cyclin-dependent kinase-1 and in cells using M110C-GWL expressing mouse embryonic fibroblasts. These Cys-gatekeeper kinases were sensitive to **ASDO2/6**-inhibition, but not AS-kinase inhibitor 3MB-PP1 and vice versa. These compounds, with AS-kinase inhibitors, have the potential to inhibit multiple AS-kinases independently with applications in systems level and translational kinase research as well as the rational design of type II kinase inhibitors targeting endogenous kinases.

Overview of kinases and analog-sensitive kinase technology. Eukaryotic protein kinases represent one of the largest protein families in the human genome with ~520 members and constituting about 2% of all human genes[1]. These enzymes catalyze the transfer of the γ-phosphate group from ATP to serine (Ser), threonine (Thr) or tyrosine residues on their substrate proteins or peptides. This post-translational modification is a critical and nearly ubiquitous mode of intracellular signaling, with about 30% of all proteins being phosphorylated[2, 3]. It is, therefore, to no surprise that aberrant expression and activation of this class of proteins often leads to a variety of diseases with about 244 kinases mapping to disease loci and cancer amplicons[1, 4, 5].

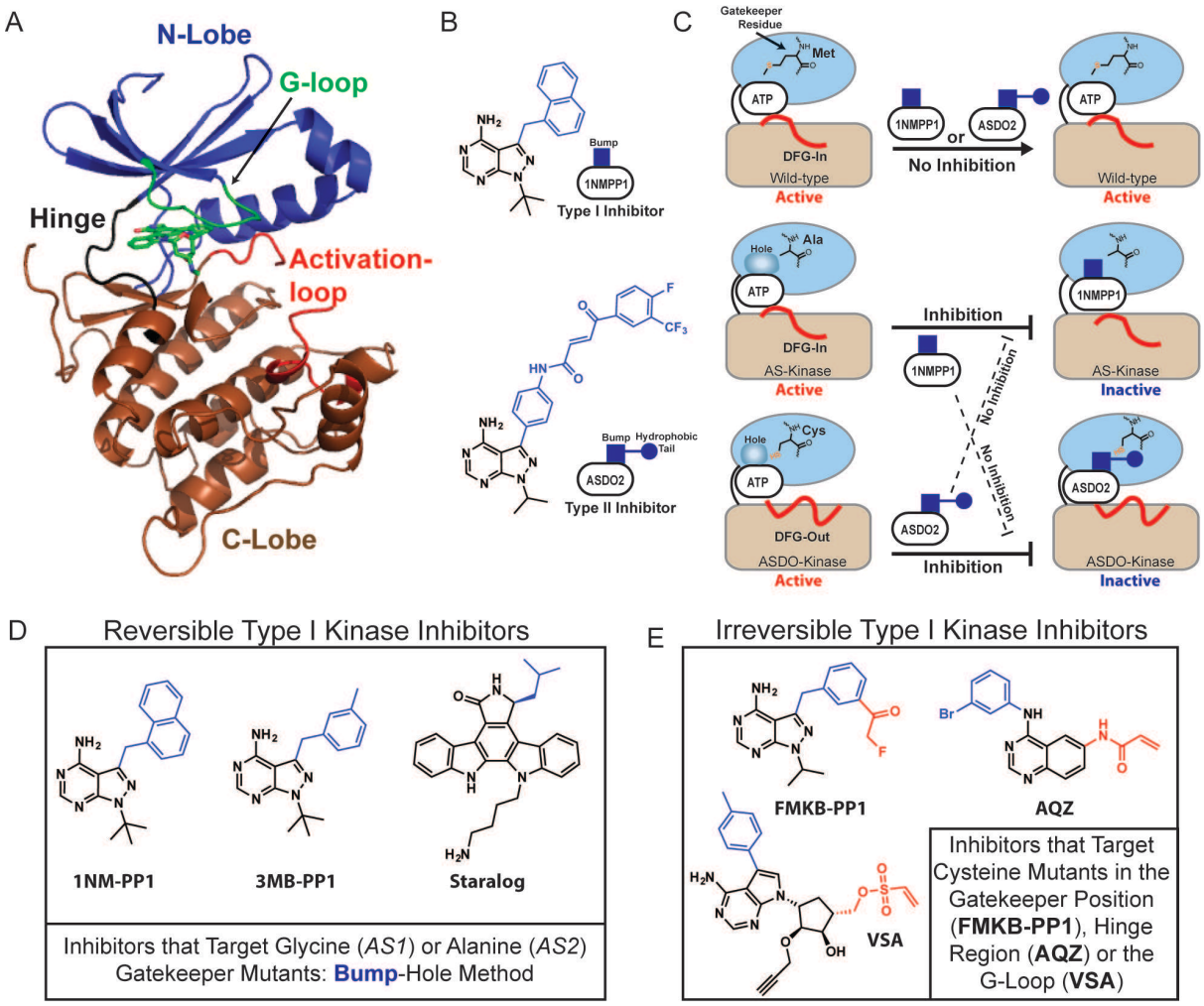

Figure 1. AS- and ASDO-kinase systems. **A**) Tertiary structure of the Staurosporine-bound GWL domain with key features highlighted (PDB: 5LOH). **B**) Chemical structures of 1NM-PP1 and ASDO2. **C**) Cartoon depicting a wild type kinase (top) with a bulky methionine gatekeeper residue. Mutating the gatekeeper residue to a smaller alanine (or glycine) residue generates an analog-sensitive (AS) kinase (middle). Mutating the gatekeeper residue to a cysteine generates an AS-kinase that is susceptible to inhibition by novel 'DFG-out' conformation-targeting inhibitors (**ASDOs; ASDO2** depicted here, bottom). The AS- and ASDO-kinase

systems are orthogonal to wild type kinases and each other. **D**) A panel of reversible type I inhibitors that target alanine- or glycine-gatekeeper mutants. **E**) A panel of irreversible type I inhibitors that target cysteine mutations in the gatekeeper, hinge or G-loop regions. Structural features highlighted in **BLUE** complement the expanded hydrophobic pocket that is generated by mutation of the gatekeeper residue to alanine or glycine and features highlighted in **RED** represent cysteine-reactive, electrophilic warheads (fluoromethylketone, acrylamide and vinylsulfone).

One way to study kinase function and manage dysregulated kinases is through development of selective kinase inhibitors; however, due to the high degree of structural similarity, particularly in and around the ATP-binding pocket, it is often difficult to target an individual kinase with small-molecule inhibitors. One way to circumvent this issue is by employing a chemical-genetic strategy that takes advantage of a structurally conserved, mostly hydrophobic residue within the kinase active-site, termed the gatekeeper residue[6-8]. Mutation of this residue from a normally bulky residue to a smaller one, such as alanine (Ala) or glycine (Gly), engenders an analog-sensitive (AS) kinase containing a unique binding-site that can be exploited pharmacologically with bulky ATP-analogs such as 1NM-PP1[8], 3MB-PP1[8] and the recently developed staralogs[7] (Figure 1A-D). This 'bump-hole' method has been utilized for the study of at least 85 different kinases, yet despite this level of success there are still a number of kinases, coined 'intolerant' kinases, that do not tolerate gatekeeper mutations[8-11]. To expand the scope of AS-technology, researchers have identified second-site mutations, or suppressor of Gly gatekeeper mutations (*sogg*), that restore the kinase activity to some 'intolerant' AS-kinases (applied to at least 11 kinases so far) when the gatekeeper is Gly or Ala[8, 10]. In addition, electrophile-sensitive (ES)-kinases can be selectively inhibited by electrophilic, bulky PP1- or ATP-analogs (Figure 1E) (*e.g.* fluoromethylketobenzyl (FMKB)-PP1, acrylamido-anilinoquinazolines (AQZ) and 5'-vinylsulfonyl adenosine (VSA)) by targeting cysteine (Cys)-mutations within the gatekeeper or other positions vicinal to the ATP-binding pocket (*i.e.* in the Gly-rich loop (G-loop) or hinge region, Figure 1A)[9, 12-18]. However, these approaches appear to be highly specific to individual kinases and not widely applicable. This also limits the possibility to differentially inhibit two kinases with two orthogonal chemical genetic systems. Such a dual bio-orthogonal approach would be ideal for investigating kinase signaling crosstalk, synthetic lethality and many other areas of systems biology and translational research across a diverse set of kinase drug targets.

In this study, we report the development of a new chemical-genetic approach based on a Cys-gatekeeper mutation and non-covalent, type II mode of kinase inhibition that targets the inactive "DFG-out" kinase conformation (Figure 1)[19]. We verified this approach with three

divergent Ser/Thr-kinases: Greatwall kinase (GWL), Aurora-A kinase (AAK) and Cyclin-dependent kinase-1 (Cdk1). To demonstrate compound efficacy in cells, we measured substrate phosphorylation and cellular proliferation, a phenotype functionally linked to GWL activity[20, 21], in wild type (WT)- and M110C (MC)-GWL expressing mouse embryonic fibroblasts (MEFs). **ASDO2** (**A**nalog-**S**ensitive "**D**FG-**O**ut" kinase inhibitor-**2**) specifically inhibited phosphorylation of the physiologic GWL substrate α-endosulfine[22] (ENSA) and attenuated proliferation in MC-GWL expressing MEFs, but not in WT-GWL expressing cells. Together, these data support expanding the AS-kinase inhibitor tool set with "DFG-out" targeting **ASDO** inhibitors, which in combination allow for the independent targeting of at least two distinct kinases (Figure 1C).

RESULTS AND DISCUSSION

Approaches utilized to expand analog-sensitive kinase technology. The starting point of this study was an effort to develop an AS-version of microtubule-associated Ser/Thr kinase-like (MASTL) protein, commonly known as GWL, in order to investigate its mitotic functions and role in the cell cycle[23]. Over-expression and immunoprecipitation of FLAG-tagged GWL constructs provided a means to assess the activity of a cohort of GWL mutants (Figure 2A). This assay demonstrated that GWL is an 'intolerant' kinase evidenced by the inactivity of the *AS1* (M110G) and *AS2* (M110A) GWL kinase alleles (Figures 2B-C & S1A), and neither *sogg* mutations nor the ES-kinase approach were capable of generating an AS-GWL system (Figure S1A-G). In the first instance, we decided to make *sogg* mutations at the analogous positions in GWL, which included mutations that were previously successful for kinases such as Pto (L68I), APH(3')-IIIa (N268T) and GRK2 (S268V) (Figure S1G)[10]. Only one of these mutations, V61I-GWL, augmented GWL activity, evidenced by increased myelin basic protein phosphorylation, but did not restore activity of the double mutant V61I/M110A-GWL (Figure S1B). Bioinformatically, we identified sites in the G-loop consensus sequence (GxGxxG) that deviated from other AGC kinases, but reversion mutations in the G-loop, made to adopt the more common amino acids, had a meagre (S42G) to no (S42G/A45S) effect in combination with M110A-GWL (Figure S1A-C)[24].

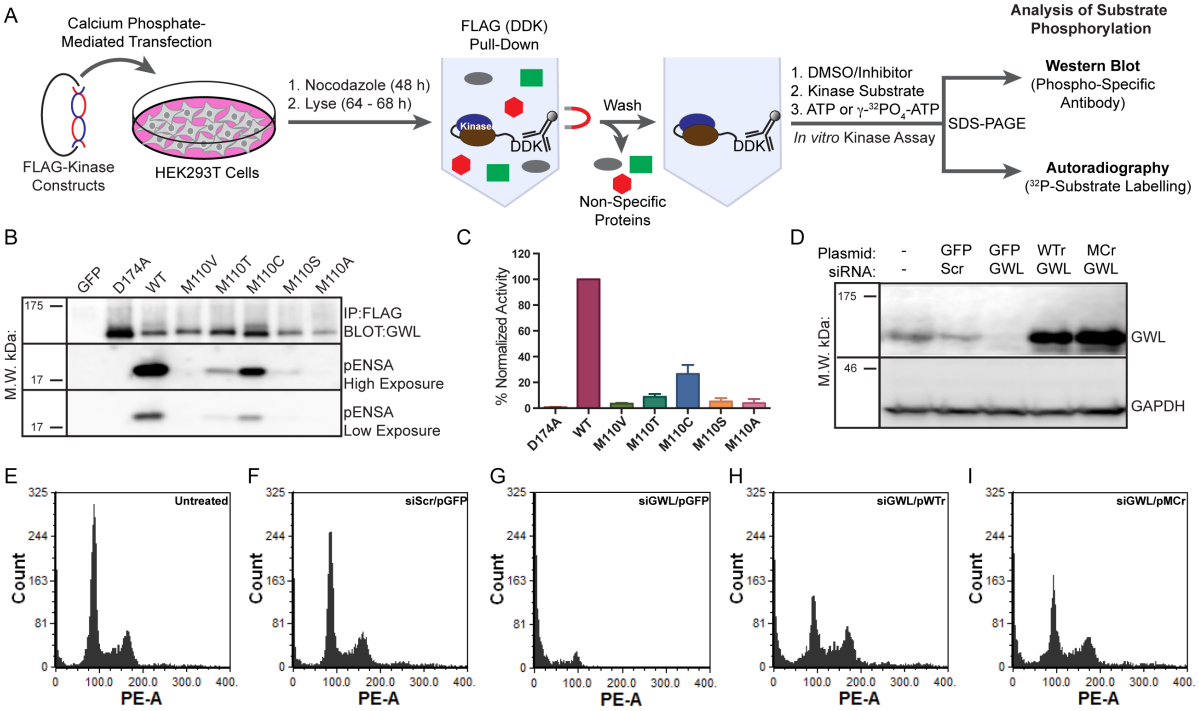

Figure 2. Systematic mutational analysis of the GWL gatekeeper position. A) General workflow for the immunoprecipitation-mediated kinase assay. **B,C**) Systematic analysis of gatekeeper mutations in the GWL ATP-binding pocket. **D**) Rescue of RNAi-mediated GWL depletion by co-expression with siRNA-resistant WT- and MC-GWL constructs (WTr- and MCr-GWL). **E-I**) FACS-cell cycle analysis of HeLa cells. Kinase assays were performed at least 3-times per mutation and quantitation using ImageJ (1.47v) (densitometry) of the average normalized % kinase activity (pENSA:GWL ratio used as a readout of kinase activity) ± S.D. was performed and plotted using Prism 6.0.

Initial efforts to identify *sogg* mutations for Ala-gatekeeper GWL were unsuccessful, and thus we hypothesized that other small amino acids, presumably preserving an expanded hydrophobic ATP-binding pocket, might be useful in combination with previously identified or new *sogg* mutations. To explore this idea further, the gatekeeper position was scanned with relatively small amino acids, which led to the discovery that MC-GWL-mediated phosphorylation of ENSA was only 4-fold less compared to WT (Figure 2B – C). Furthermore, through FACS analysis, we showed that RNAi-resistant MC-GWL, unlike M110A-GWL, was able to restore G_1, S and G_2/M cellular levels to the same extent as an siRNA-resistant WT rescuing plasmid in GWL depleted HeLa cells (Figures 2D – I & S2A – F). This result inspired the generation of an ES-kinase system; however, the electrophilic inhibitors AG1-2 and FMKB-PP1 (Figures 1E, S1D & E and S2), which were validated against T338C-c-Src, did not robustly inhibit MC-GWL at 20 μM concentrations (Figure S1D – E)[9]. Of the other small gatekeeper mutations, M110T-GWL displayed ~8% activity compared to WT, and thus we

made Cys mutations in an M110T-GWL mutant to mimic the cysteines in the hinge regions of EphB3 (C717) and EGFR (C797); M110T/G116C and M110T/D117C[13, 15]. In combination with a Thr gatekeeper, similar mutations in EphB1 (G703C) and c-Src (S345C), to name a few, are targetable using electrophilic quinazoline-based inhibitors (*e.g.* AQZ, Figure 1D), but due to the inactivity of these GWL double mutants, we were not able to apply them (Figure S1F – G)[13, 15].

AD57-analogs specifically target MC-GWL *in vitro*. Due to the inefficacy of known ES-kinase inhibitors against MC-GWL, we decided to generate novel inhibitors based on the structure of AD57[25] (Figures 3A & S3). We surmised that replacement of the urea linker with an acrylamide linker might allow selective targeting by a nucleophilic Cys-mutant[16]. AD57 also seemed like an ideal candidate as it selectively inhibited MC-GWL with an IC_{50} value of 10.6 ± 0.4 μM and displayed no inhibitory activity against WT-GWL (Figure 3B & D). **ASDO1**, the first in a series of AD57-analogs, was synthesized by coupling of an anilinopyrazolopyrimidine with a 3-benzoylacrylic acid chloride (Supplemental Schemes 1 – 3 & Fig. 4A)[9, 26]. The resulting compound contained an acrylamide linker bridging the pyrazolopyrimidine moiety with a trifluoromethylbenzoyl group. This feature is similar to a trifluoromethylphenyl group, which is commonly incorporated into some type II kinase inhibitors[19, 27]. **ASDO1** (**A**nalog-**S**ensitive "**D**FG-**O**ut" kinase inhibitor-**1**) (Figure 3A) completely abrogated MC-GWL activity at a concentration of 20 μM without inhibiting WT-GWL (Figure S3). By assaying AD57 and **ASDO1** more rigorously using the immunoprecipitation-based kinase assay with ENSA as substrate, we were able to show that **ASDO1** exhibited a >60-fold improvement in potency against MC-GWL with an IC_{50} value of 0.17 ± 0.09 μM and remained exquisitely selective for MC- vs. WT-GWL even up to concentrations as high as 100 μM (Figures 3C – D, 4A & S4A – B).

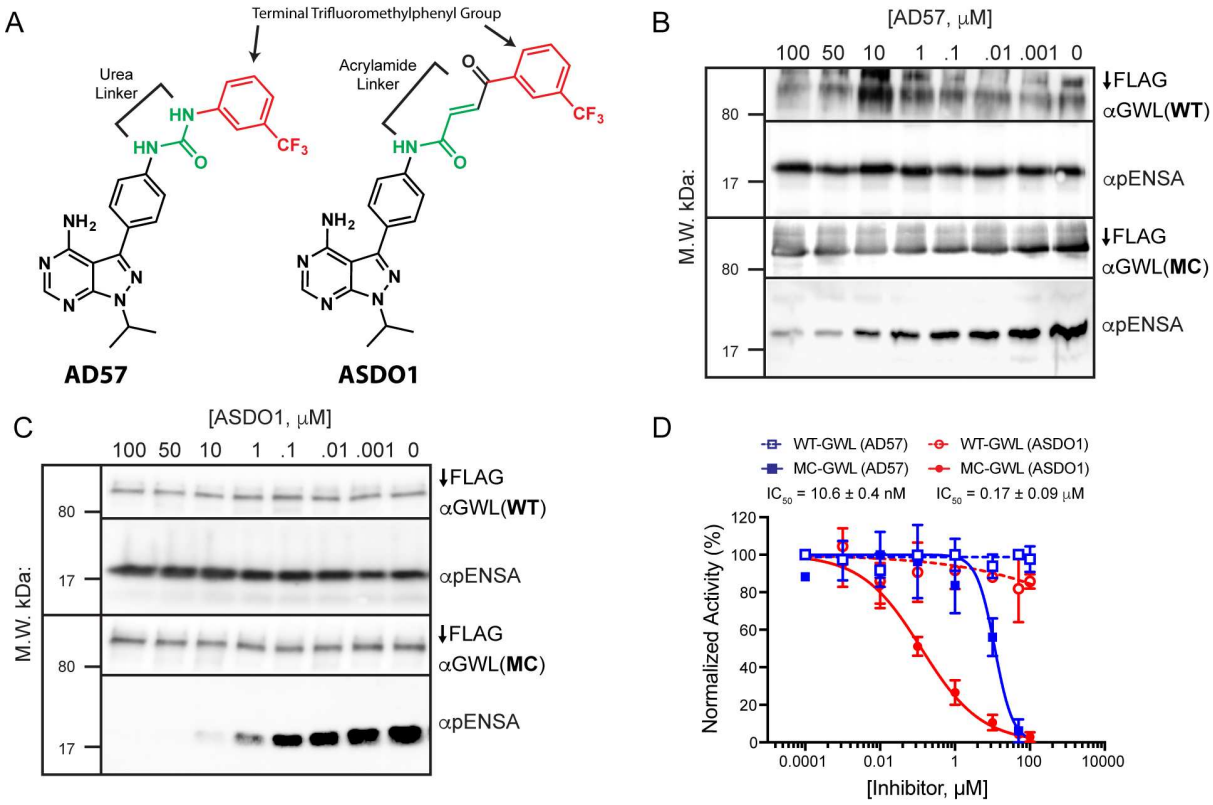

Figure 3. Establishing the inhibitory activity of AD57 and ASDO1 in the GWL kinase assay. A) Chemical Structures of AD57 and **ASDO1**. Structural features highlighted in **Green** are linkers that bridge the PP1 moiety with the terminal trifluoromethylphenyl (**Red**) group. **B-C**) FLAG-tagged WT- and MC-GWL kinase assays in the presence of increasing concentrations of AD57 (**B**) or **ASDO1** (**C**). **D**) Kinase activity was quantitated using ImageJ (1.47v) (densitometry) and reported as the average normalized % kinase activity ± S.D.

Structural studies using an AD57-c-Src co-crystal structure predicted that formal halogenation of the terminal phenyl ring with *ortho*-fluorine and *para*-chlorine substituents would fine-tune the selectivity profile of AD57. Indeed, these halogenated AD57-derivatives maintained inhibitory activity toward Ret, Raf, Src and S6K, reduced mTor inhibition and led to significantly less toxicity in a multiple endocrine neoplasia type 2 *Drosophila* model system[25]. In an attempt to fine-tune the selectivity of **ASDO1** toward MC- vs. WT-GWL, we synthesized halogenated and bulkier, non-halogenated **ASDO**-derivatives by first incorporating acetophenones into the microwave-assisted aldol-condensation with glyoxylic acid to yield 3-benzoylacrylic acids[26], which after conversion to acid chlorides were later coupled with anilinopyrazolopyrimidines (Supplemental Schemes 2 – 3 & Figure 4A) to produce **ASDOs 2** – **6**.

ASDO2 contains a trifluoromethylbenzoyl group with a *para*-fluoro substituent and demonstrated an ~3-fold improvement in potency, whereas the effect of the *para*-chloro substitution (**ASDO3**) was negligible (Figures 4A – C & S4C – E). We also explored the activity of bulkier derivatives in hopes of improving their selectivity for Cys-gatekeeper versus WT kinases. Unfortunately, replacing the central benzene ring with a naphthyl (**ASDO4,** Figures 4A & S4F) or 3-methylbenzyl group (**ASDO5,** Figures 4A & S4G) dramatically weakened inhibitory activity; however, the 2-methylphenyl substitution of the inner-benzene ring (**ASDO6**) in combination with the *para*-fluoro substitution seen in **ASDO2** resulted in a compound with inhibitory activity almost equal to that of the **ASDO1** precursor (Figures 4A, C – D & S4H – I). Interestingly, **DO1**, which lacks the pyrazolopyrimidine group, also displayed mono-specific targeting of MC-GWL vs. WT, but with attenuated inhibitory activity compared to **ASDO1** (Figures 4A, C & S4J – K), suggesting that the selectivity filter resulting in Cys-gatekeeper kinase specificity lies within the phenylbenzoylacrylamide scaffold and that the electrophilic olefin might be targeted by the Cys-gatekeeper residue. Furthermore, replacement of the trifluoromethyl group of **DO1** with a *para*-ethoxy substituent (**DO2**) completely ablated inhibitory activity toward both WT- and MC-GWL (Figures 4A, C & S4L – M). Interestingly, some type II kinase inhibitors (*e.g.* AD57 and Sorafenib[25, 27]) possess a trifluoromethyl substituent on their terminal phenyl ring, which occupies space in an allosteric hydrophobic pocket unique to the inactive kinase conformation[19, 28]. In contrast to **DO1**, the lack of inhibitory activity of **DO2** hints at the possibility that this series of compounds, like the parent compound AD57, might stabilize the inactive 'DFG-out' kinase conformation.

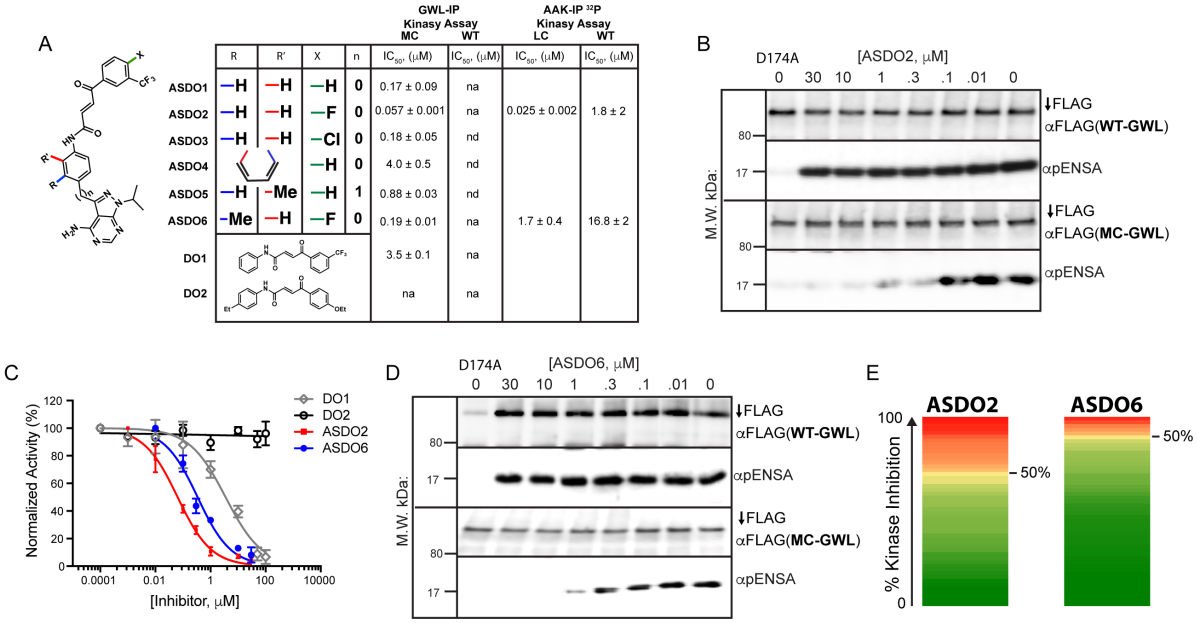

Figure 4. *In vitro* analysis of ASDO-derivatives. A) The potency of synthetic AD57-derivatives (**ASDOs**), **DO1** and commercially available **DO2** was assessed using an *in vitro* immunoprecipitation kinase assay; na = not applicable and nd = not determined. The

potencies of **ASDO2** (**B-C**) and **ASDO6** (**C-D**) were determined using FLAG-tagged WT- and MC-GWL kinase assays. **E**) **ASDO2** and **ASDO6** were screened at 1μM against a panel of 50 kinases, carefully selected to represent the kinome, using the Kinase Express Screen (International Centre for Kinase Profiling, University of Dundee).

To establish the importance of the bulkier central ring of **ASDO6**, both **ASDO2** & **6** were subjected to a rigorous kinase inhibition-profiling screen (International Centre for Kinase Profiling, University of Dundee Kinase Profiling Express Screen). At 1 μM, **ASDO2** inhibited 15 of 50 kinases with inhibitory activity ≥ 60% (60 – 95%); however, as is the case with classical AS-kinase inhibitors, the increased bulk of the central benzene ring of **ASDO6** likely accounts for the decrease in number of WT-kinases targeted with inhibitory activity > 60% (62 – 84%); only 4 of 50 kinases. Note that the higher end of the inhibitory range decreased from 95% for **ASDO2** to 84% for **ASDO6**, providing further evidence that the bulkier **ASDO6**-derivative is more refractory toward WT-kinases (Figures 4E & S5A – B).

ASDO6 targets AAK and Cdk1 bearing a Cys-gatekeeper and displays orthogonality with WT kinases. Next, we sought to place **ASDO**-compounds within the pantheon of general AS-kinase inhibitors. To do this, we mutated the gatekeeper positions of AAK (L210) and *Xenopus laevis* Cdk1 (F80) to cysteines and subjected them to kinase assays with increasing concentrations of **ASDO2** and/or **6** (Figures 5A – F & S6A – C). Both kinases tolerated the Cys-gatekeeper mutation with improved (Cdk1) or a slight reduction (AAK) in kinase activity compared to WT (Figure S6B – C). Moreover, **ASDO2** inhibited L210C (LC)-AAK with the greatest potency, demonstrating an IC_{50} value of 25 ± 2 nM (Figures 4A, 5A & C) and was >70-fold selective in targeting LC-AAK vs. WT-AAK. Although less potent than **ASDO2**, **ASDO6** inhibition of LC-AAK (IC_{50} = 1.7 ± 0.4 μM) and F80C-Cdk1 was about 10-fold more selective vs. their WT counterparts, respectively (Figure 5B – F).

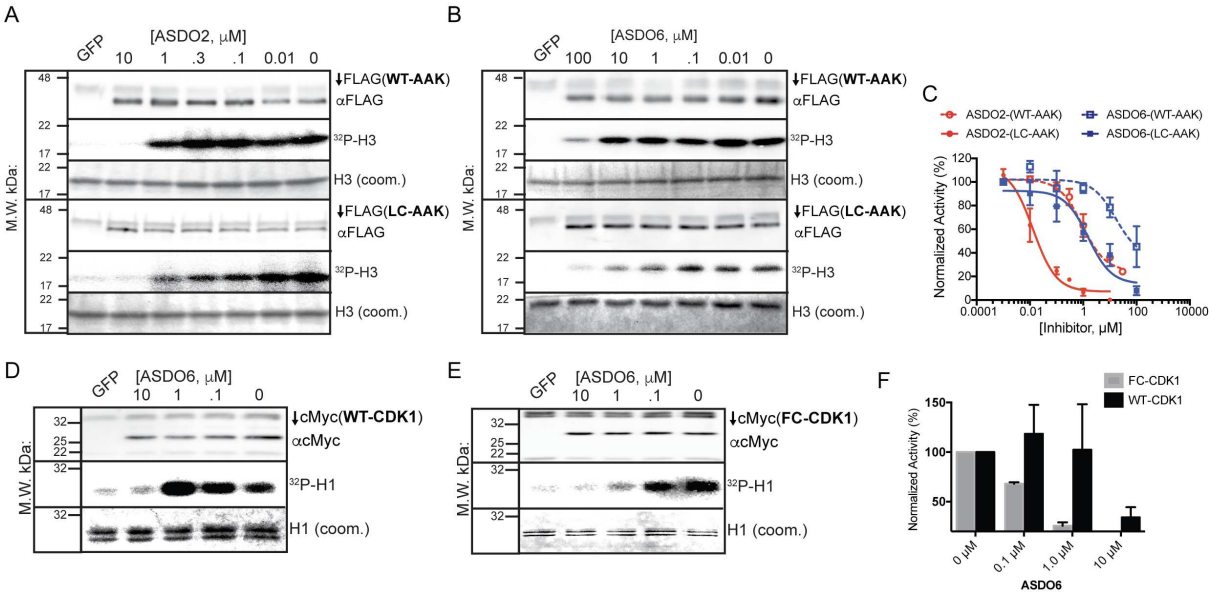

Figure 5. *In vitro* analysis of ASDO2/6 in FLAG-AAK and Myc-Cdk1 kinase assays. The inhibitory activity of **ASDO2** (**A&C**) & **ASDO6** (**B-C**) against FLAG-tagged WT- and LC-AAK constructs was assessed using a radioactive kinase assay to detect $^{32}PO_4$-H3 substrate. **D-E)** The inhibitory activity of **ASDO6** against MYC-tagged WT and F80C-Cdk1 was assessed using a radioactive kinase assay for the detection of $^{32}PO_4$-H1. **C,F**) Kinase activity was quantitated using ImageJ (1.47v) (densitometry) and reported as the average normalized % kinase activity ± S.D.

ASDO2 selectively inhibits MC-GWL in cells. Although **ASDO6** inhibited less WT-kinases with inhibitory activity >60% (Figure 4E), **ASDO2** displayed greater potency and specificity in GWL and AAK kinase assays (Figure 4A). We, therefore, opted to assess the effects of **ASDO2** on cellular ENSA phosphorylation and proliferation in MEFs over-expressing WT- or MC-GWL. To establish cellular models for MC-GWL, we decided to employ MEFs containing loxP sites flanking exon 4 of the murine GWL gene[29]. Treatment of these cells with Cre-expressing adenovirus depleted GWL and allowed for reintroduction of human WT- or MC-GWL cDNA via lentiviral transduction (Figure 6A). After confirming the presence of human GWL by western analysis, both populations of WT- and MC-GWL expressing cells were treated with nocodazole (200 ng/mL) for 16 – 20 h (Figure 6B). The activity of mitotic kinases increases substantially during mitosis, making the nocodazole-mediated mitotic arrest (M-arrest) essential for visualizing the cellular inhibition of ENSA phosphorylation; inhibition of an inactive kinase would only reveal background level phosphorylation. After M-arrest and 4 h of 2 μM **ASDO2** or DMSO treatment, cells were harvested, lysed and probed with anti-phospho-ENSA (pENSA) antibody by western blot analysis, revealing mono-specific inhibition of MC-GWL-mediated ENSA phosphorylation (Figure 6C – D). Functionally, GWL has been linked to cellular proliferation in several studies, and thus serves as an ideal gauge for GWL activity[20,

[21]. After 5 d of growth in the presence of inhibitor or DMSO, we observed that only cells depleted of endogenous WT-GWL and over-expressing MC-GWL had dramatically reduced proliferation in an **ASDO2** concentration-dependent manner, thus confirming the utility of **ASDO2** and possibly other **ASDO**-derivatives in cellular models (Figure 6E).

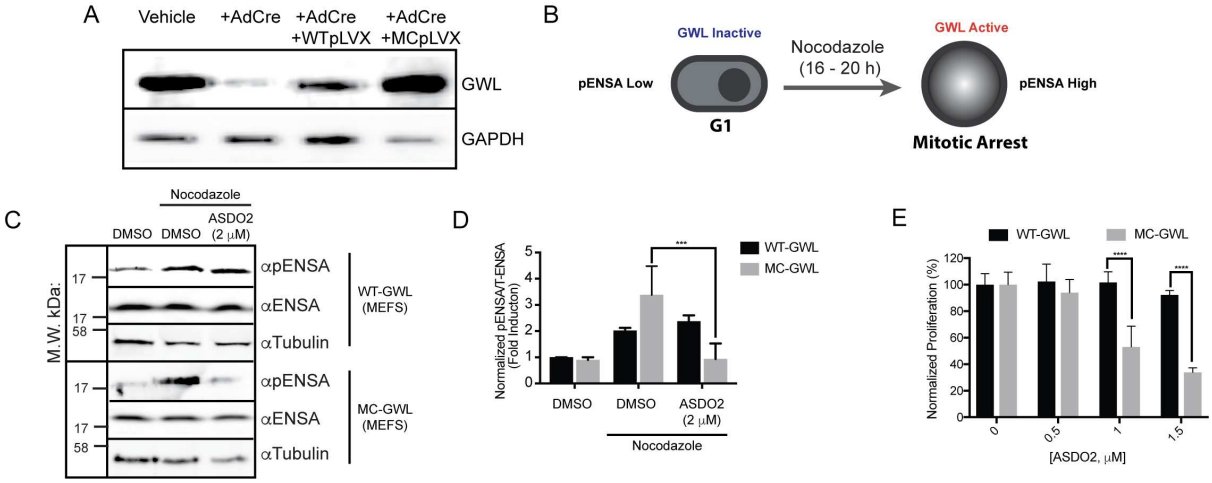

Figure 6. Cellular analysis of ASDO2 in WT- and MC-GWL expressing mouse embryonic fibroblasts (MEFs). A) Expression of exogenous WT- and MC-GWL confirmed by western analysis. **B**) Strategy used to fully activate GWL in MEFs. Cells were treated with 200 ng/mL nocodazole for 16 – 20 h before harvesting for downstream applications. **C-D**) Mitotic cells were treated with 2μM **ASDO2** or DMSO for 4 h. ENSA, phospho-ENSA and tubulin levels in cell lysates were determined by western analysis. All experiments were repeated thrice and activity (pENSA:ENSA ratio) was quantitated using ImageJ (1.47v) (densitometry), normalized to DMSO control and reported as the average fold induction relative to DMSO control (without nocodazole) ± S.D. **E**) CellTiter Blue Proliferation assays.

ASDO2 displays relatively slow-on and -off kinetics. At this point, it was still unclear how **ASDO2/6** mono-specifically targeted MC- vs. WT-GWL (*i.e.* as a type I or II inhibitor) and the presence of an electrophilic, doubly-activated olefin brings to question whether or not it interacts with MC-GWL in a reversible or irreversible manner. To further probe the mechanism of action of **ASDO2**, we investigated the reversibility of inhibition in comparison to a type I inhibitor (staurosporine) and the parent type II inhibitor AD57; note that type I inhibitors generally display fast-on/fast-off binding/dissociation kinetics, whereas type II inhibitors generally display slow-on/slow-off binding/dissociation kinetics[28, 30].

Initially, a washout experiment with MC-GWL supported the notion of an ES-kinase model system. Evidence for this is seen by the failure of **ASDO2**-treated (10 μM) MC-GWL to regain activity after 5 washes over a 4 h period compared to the quick reactivation of staurosporine (STP)-treated (50 μM) MC-GWL under the same conditions (Figure 7A – C). However, when

we probed reactivation of MC-GWL after longer periods of time following washout of **ASDO2** and AD57 (*bona fide* type II inhibitor), it became evident that MC-GWL regained activity over time, but this reactivation period took longer due to a relatively slower off-rate (Figure 7D – E). Importantly, activity may not have rebounded to levels demonstrated by fully active MC-GWL (not treated with inhibitor) due to decomposition or destabilization of the protein over a 24 h period. Additionally, **ASDO2** rapidly inhibited MC-GWL activity, but with a slight difference in inhibitory activity between 20- and 60-minute compound pre-incubation periods (Figure 7F). Taken together, these data suggest that **ASDO2** shares similar slow-off binding-kinetics as the type II inhibitor AD57, but could also be acting, to a small extent, in an irreversible manner as inhibition marginally improves over time (Figure 7F). Unfortunately, expression, purification and X-ray crystallography of full-length GWL has proven to be a major technical challenge; therefore, to pin down the exact binding mode of **ASDOs** in GWL, technical innovations in GWL structural biology are required[20].

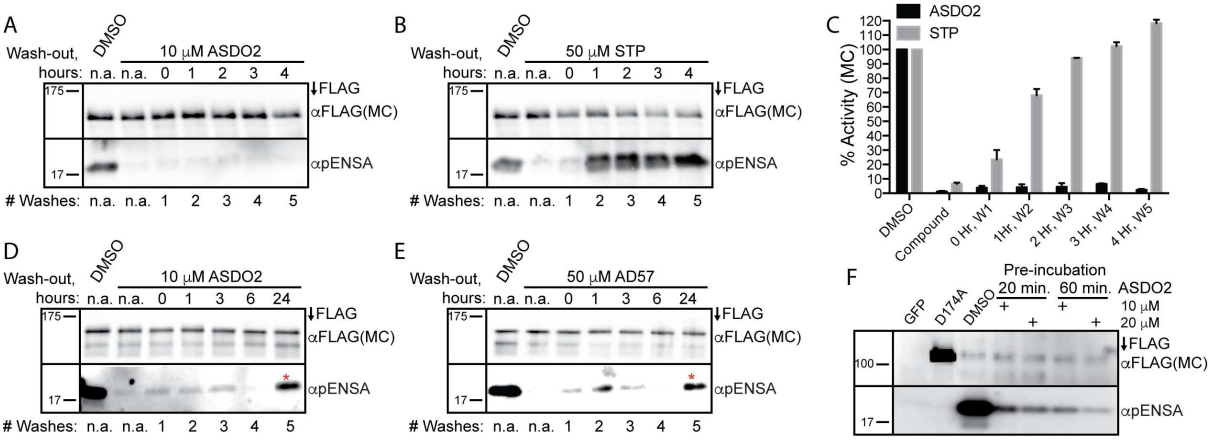

Figure 7. Comparing binding kinetics of ASDO2 to type I/II kinase inhibitors staurosporine (STP, type I) and AD57 (type II). FLAG-tagged MC-GWL was treated with DMSO (**A – F**), **ASDO2** (**A,C & D**), STP (**B,C**) or AD57 (**E**) for 20 minutes and then subjected to GWL kinase assay conditions. These beads were also subjected to several washes (buffer exchange) for the indicated amount of time before start of the kinase assay (**A – F**). **F**) Kinases assays were performed with FLAG-tagged MC-GWL, pre-incubated with DMSO or **ASDO2** for 20 or 60 m before start of the kinase reaction; reaction started by addition of ATP and ENSA. All experiments were repeated thrice and the average pENSA/FLAG(M110C-GWL) ratio was quantitated using ImageJ (1.47v) (densitometry) and normalised to DMSO control (**C**).

ASDO2/6 demonstrates a type II inhibitor binding mode with LC-AAK. To cement the binding-mode of **ASDO2/6**, we solved X-ray co-crystal structures with LC-AAK[31]. Both compounds were sandwiched between the N- and C-terminal lobes bound to the ATP-binding pocket, making the expected interactions with the backbone of the hinge region (Glu211 and

Ala213) and stretching all the way to the Cα-helix, displacing it in comparison to the WT-AAK ADP-bound structure (PDB: 4CEG, Figure S7A – D). In both cases, the DFG-motif aspartic acid residue adopts an 'out' conformation (DFG-out), in which Phe275 points into the ATP-binding pocket, while the terminal aromatic groups of both compounds are buried in hydrophobic pockets adjacent to the Cα-helix, indicative of type II kinase inhibitors (Figures 8A, B & S6D)[19]. In fact, overlay of the Asp274 residues of the 1NM-PP1- (type I, PDB: 4LGH) and **ASDO2/6-** (type II) bound structures illustrates a key difference between type I and II inhibitors: The Asp residue flips 180° going from an active to an inactive conformation, allowing Phe to pack against **ASDO6** (Figures 8A, B & S7D).

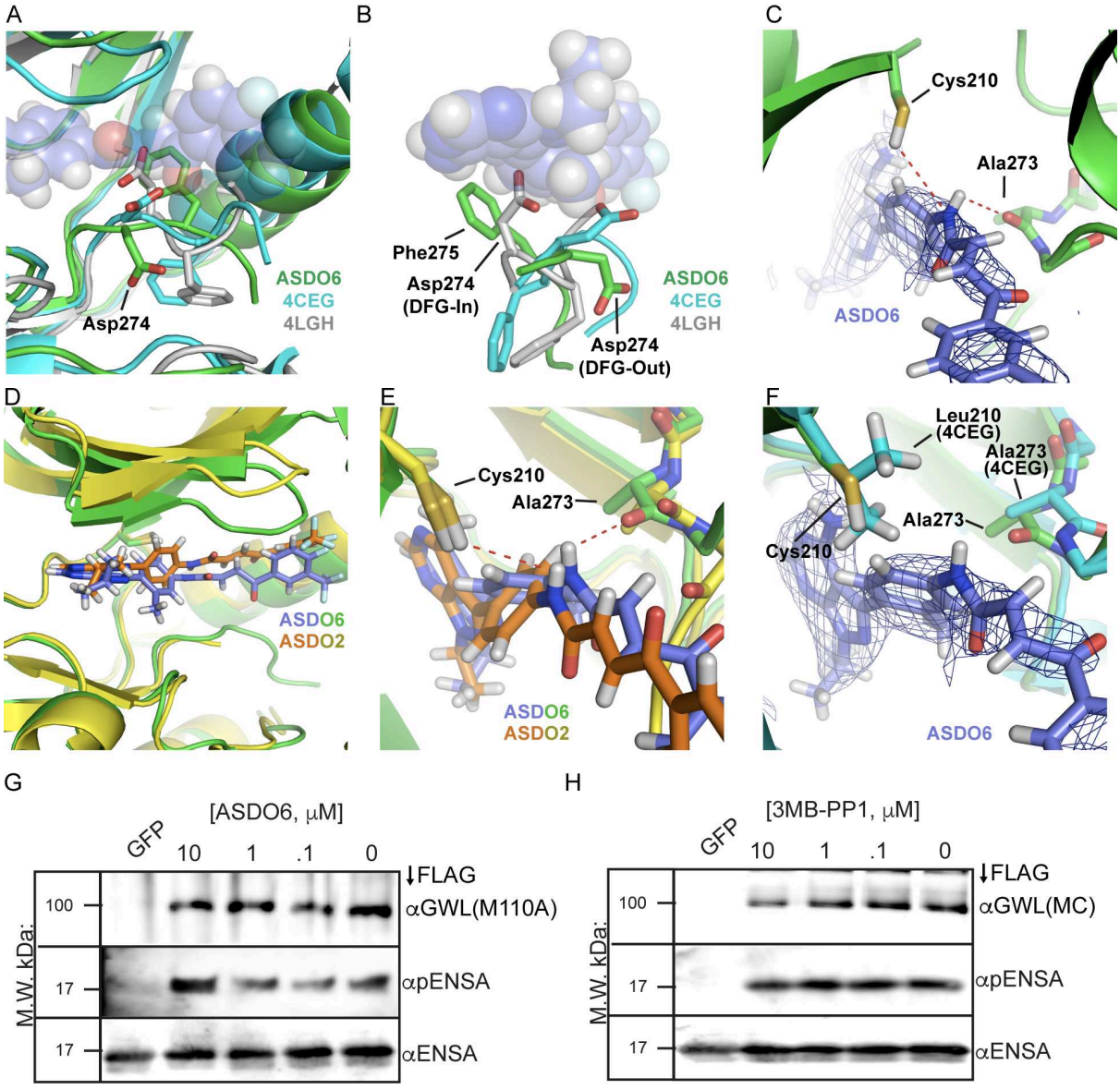

Figure 8. X-ray co-crystal structures of ASDO2 and ASDO6 with LC Aurora-A kinase. A) Alignment of **ASDO6**, ADP (4CEG) and 1NM-PP1 (4LGH) bound structures reveals the orientation of their respective catalytic-motif aspartic acid residues. **B**) A zoomed-in view of

panel (**A**). **C**) **ASDO6** abuts the gatekeeper cysteine residue forming a weak electrostatic interaction with the thiol hydrogen of cysteine and a stronger hydrogen-bonding interaction with the backbone of Ala273, serving to clamp **ASDO6** within the nucleotide binding-site proximal to the gatekeeper position. **D**) Comparison of the **ASDO2**- and **ASDO6**-bound LC-AAK structures. **E**) A zoomed-in view of panel (**D**). **F**) Superimposition of the **ASDO6**- and ADP-bound structures reveals a potential conflict between the **ASDO6**-amide and the hydrophobic L210 gatekeeper residue. **G,H**) **ASDO6** (**G**) and 3MB-PP1 (**H**) inhibitory activity was assessed against M110A-GWL and MC-GWL respectively using the immunoprecipitation kinase assay.

In the **ASDO6**-bound structure, Cys210 appears to form a weak, electrostatic interaction with the amide 'N', and the Ala273 backbone carbonyl forms a strong hydrogen bond with the same amide group, serving as a molecular clamp that also brings to light the importance of the cysteine residue (Figure 8C). Comparing the **ASDO2-** and **6-**bound structures also sheds light on the molecular level basis for the decrease in WT-kinase targeting by **ASDO6**; that **ASDO6** prefers binding to AAK only when the gatekeeper residue is a polar amino acid such as cysteine. Alignment of these structures shows that the methylphenyl ring of **ASDO6** twists in the direction of Cys210, bringing the amide closer to the Ala273 backbone; however, a water molecule fills the gap between **ASDO2**, Cys210 and the Ala273 backbone with all three elements forming a hydrogen-bonding network in the **ASDO2**-bound structure (Figures 8D, E & S7E).

As a result of placing the polar amide group of **ASDO6** in closer proximity to the gatekeeper residue, WT AAK, which harbors a hydrophobic Leu210 gatekeeper residue, would disfavor and destabilize the **ASDO6**-bound conformation (Figure 8F). Based on this hypothesis, other hydrophobic amino acids such as Ala should also attenuate **ASDO6** inhibitory activity and replacing cysteine with a less polar amino acid or with Gly, which lacks a side-chain, should abolish the molecular clamp mechanism and abrogate the **ASDO6**-GWL interaction as well. To test these hypotheses, we over-expressed, immunoprecipitated and treated FLAG-M110A-GWL with **ASDO6** up to a concentration of 10 μM. As predicted, **ASDO6** was not able to inhibit M110A-GWL, nor was 3MB-PP1 able to inhibit M110C-GWL *in vitro* (Figure 8G & H), suggesting the two systems work independently of each other and could be used to differentially inhibit other combinations of kinases based on gatekeeper mutations to either cysteine or Ala/Gly.

Discussion and Conclusions

AS-kinase technology has been employed to dissect the cellular functions of individual kinases across the kinase family, but there are still a number of kinases that remain averse to this methodology. In order to apply AS-kinase technology, mutations that engender sensitivity to pharmacologic inhibition must also maintain sufficient kinase activity so that the mutant kinase can recapitulate WT cellular function. There are many ways to broaden the scope of AS-kinase technology such as making *sogg* mutations that rescues the activity of 'intolerant' kinases when an Ala/Gly-gatekeeper mutation is present[10]. Also, over the years, a number of different AS- and ES-systems have been developed that incorporate amino acids other than Ala or Gly, *e.g.* Cys or Thr[9, 13, 17, 18], into the gatekeeper position, but so far, these systems have not been widely utilized in the field; though some are still in their infancy. In terms of AS-systems that have proven fruitful, a number of new reagents such as staralogs[7] offer even greater specificity and potency, but to expand the scope of AS-kinase technology further we need not focus solely on engineering inhibitors against the active kinase conformation, but take full advantage of all modes of pharmacologic inhibition. To date, type II inhibitors have been left out of the loop when it comes to the development of chemogenomic technology, but this study is the first to provide an example of a chemical genetic system based on Cys-mutant kinase inhibition with a type II inhibitor; a system that we now refer to as the **ASDO** (**A**nalog-**S**ensitive '**D**FG-**O**ut')-kinase system (Figure 1B & C).

Furthermore, type I and II kinase inhibitors bind to disparate kinase conformations resulting in their catalytic inactivation[19, 27, 28]. Due to evolutionary pressure to preserve the catalytically active kinase conformation, type I inhibitors encounter a very similar ATP-binding pocket across the kinome, made exploitable through the 'bump-hole' method. The inactive kinase conformation is not bound by this evolutionary pressure and is more varied[28], which may have hampered previous attempts to generate a type II inhibitor-based **ASDO**-kinase system. Despite this variability, we systematically optimized the **ASDO**-scaffold to engender a small-molecule inhibitor that displays generality across at least three divergent Ser/Thr-kinases bearing a Cys-gatekeeper, so far, and **ASDO2/6** display bio-orthogonality versus WT kinases (Figures 1B & 4F). As this system not only appears to take advantage of steric complementarity, but also electrostatic interactions, to engender specificity toward Cys-gatekeeper kinases, we hypothesized that it may act independently of the canonical AS-kinase system, which is based solely on steric complementarity. This theory was validated *in vitro* and will likely change the landscape of future studies involving signaling pathways in cells and disease models. These multiple AS/ASDO-kinase systems along with the *Ele-Cys* and ES-kinase systems (systems that utilize electrophilic-quinazoline and 5'-electrophilic adenosine scaffolds) now provide an ensemble of chemical genetic tools to explore differential and independent kinase inhibition across at least two kinases in cells.

Lastly, this system exploits binding to and stabilizing the 'DFG-out' conformation of kinases and we demonstrated the tenability of isolating these **ASDO**-co-crystal structures using X-ray crystallography. To date, X-ray crystal structures of inactive kinase conformations across the kinome are sparse[19, 28], but the **ASDO** system could potentially be used to generate X-ray crystal structures of other inactive kinase conformations. This technology, therefore, has great potential to galvanize drug discovery efforts by providing new 'DFG-out' X-ray crystal structures that would assist with rational, *in silico* drug design efforts.

METHODS

Kinase Assays

Immunoprecipitation and radioactive kinase assays were carried out as published previously[20]. The catalytically dead mutant D174A-GWL was used as a control for inhibition. Aurora-A and xlCDK1 assays were carried out similarly to FLAG-GWL immunoprecipitation kinase assays. N-terminally tagged FLAG-Aurora-A[32] kinase and C-terminally tagged MYC-xlCDK1 were over-expressed in HEK 293T cells using the standard phosphate-mediated transfection method. Cdk1 assays were carried out by incubating HEK 293T lysates containing MYC-CDK1 with 4 μg of anti-c-Myc antibody and immunoprecipitation with 5 μl of Dynabeads™ Protein G (Thermofisher). To detect phosphorylated histones H1 (CDK1, Fig. S5A) and H3 (1μg/20μl reaction (AAK)) the standard kinase reaction was spiked with 0.075 MBq γ-^{32}P ATP (PerkinElmer, Seer Green, UK) per 20 μl reaction. After the reaction was stopped with 5 μl 5X SDS loading buffer and boiled for 5 min at 95 °C, the mixture was resolved via SDS-PAGE (4-15% Criterion pre-cast gels; Bio-Rad Laboratories, Hemel Hempstead, UK, or 13% SDS-polyacrylamide gels). Staining with coomassie-blue revealed ~28 and 21 kDa bands respectively that were imaged by autoradiography. All concentration-dependent kinase assays were performed thrice and quantitation of activity (Phospho-signal:kinase loading ratio) using ImageJ (1.47v) (densitometry) of the average normalised % kinase activity ± S.D. was plotted using Prism 6.0. Non-linear regression using Prism 6.0 was used to calculate IC_{50} values.

Crystallisation and Data Collection

Aurora-A (containing mutations L210C, C290A and C393A)[31] was co-crystallised with **ASDO2** and **ASDO6** by mixing purified protein (500 μM) with compound (**ASDO2**, 500 μM; **ASDO6**, 1mM) in a 1:1 protein:ligand ratio, before setting up sitting drop vapour diffusion experiments at 22 °C; where 0.25 μl of complex was mixed with 0.25 μl of crystallisation buffer and equilibrated against a well volume of 50 μl.

Crystals of Aurora-A bound to **ASDO2** were obtained in condition F6 of the PEGs II Suite (0.2 M ammonium sulfate, 0.1 M tri-sodium citrate pH 5.6, 25 % w/v polyethylene glycol 4000; Qiagen, USA) and bound to **ASDO6** in condition A1 of the JCSG+ Suite (0.2 M lithium sulfate, 0.1 M sodium acetate pH 4.5, 50 % w/v polyethylene glycol 400; Qiagen, USA). No additional cryo-protectant was added as the crystals were deemed already cryo-protected from their crystallisation conditions. The crystals were cryo-cooled in liquid nitrogen and no ice formation was observed. Diffraction data to 2.4 Å (**ASDO2**) and 2.1 Å (**ASDO6**) resolution were collected at the Diamond Light Source [DLS, Didcot, UK] on beamline I04.

Phasing, Model Building and Refinement

All diffraction data were collected at 100K. Autoprocessed datasets were generated by automatic integration of the data using the software package XDS followed by processing using the Pointless and Scala programs from the CCP4 software suite. Phases were obtained by molecular replacement using Phaser with a high resolution structure of ADP-bound Aurora-A C290A,C393A (PDB: 4CEG) used as the search model. An iterative combination of manual building in Coot and refinement with Phenix.refine produced the final model. The protein crystallised in spacegroups $P3_221$ (**ASDO2**) and $P6_122$ (**ASDO6**), with a single molecule comprising the asymmetric unit.

Table 1: Crystal data and structure refinement (**ASDO2**)

Resolution range (Å…)	76.88 - 2.4 (2.486 - 2.4)
Space group	P 32 2 1
Unit cell	88.769 88.769 77.28 90 90 120
Total reflections	28217 (2745)
Unique reflections	14112 (1373)
Multiplicity	2.0 (2.0)
Completeness (%)	100.00 (100.00)
Mean I/sigma(I)	23.07 (4.63)
Wilson B-factor	57.84
R-merge	0.01263 (0.1532)
R-meas	0.01786
CC1/2	1 (0.93)
CC*	1 (0.982)
R-work	0.2022 (0.2668)
R-free	0.2354 (0.3553)
Number of non-hydrogen atoms	2054
macromolecules	1993
ligands	43
water	18
Protein residues	255
RMS(bonds)	0.013
RMS(angles)	1.33
Ramachandran favored (%)	90
Ramachandran outliers (%)	2.8
Clashscore	13.13
Average B-factor	74.4
macromolecules	74
ligands	97
solvent	69.2

Table 2: Crystal data and structure refinement **(ASDO6**)

Resolution range (Å…)	71.04 - 2.13 (2.206 - 2.13)
Space group	P 61 2 2
Unit cell	82.027 82.027 172.609 90 90 120
Total reflections	39980 (3856)
Unique reflections	19990 (1928)
Multiplicity	2.0 (2.0)
Completeness (%)	99.94 (99.33)
Mean I/sigma(I)	17.84 (1.51)
Wilson B-factor	44.14
R-merge	0.03359 (0.7864)
R-meas	0.0475
CC1/2	0.999 (0.427)
CC*	1 (0.774)
R-work	0.2086 (0.3889)
R-free	0.2682 (0.3975)
Number of non-hydrogen atoms	2193
macromolecules	2037
ligands	80
water	76
Protein residues	256
RMS(bonds)	0.011
RMS(angles)	1.11
Ramachandran favored (%)	96
Ramachandran outliers (%)	0.4
Clashscore	6.46
Average B-factor	60.8
macromolecules	59.7
ligands	87.9
solvent	61.6

Supplementary Figures

Supplementary figures in support of this manuscript can be found in the **Supporting Information.**

AUTHOR INFORMATION

The authors declare no competing financial interests.

PDB ACCESSION NUMBER

Authors will release the atomic coordinates upon article publication.

CORRESPONDING AUTHOR

* Cory A. Ocasio; tony.ocasio@crick.ac.uk; +44 (0)2037 963780

FUNDING

This work was funded by the European Community's Seventh Framework Programme [FP7/2007-2013] under grant agreement number PIIF-GA-2011-301062 (CAO), the Cancer Research UK Programme Award C24461/A23302 (RB) and through the MRC CASE industrial studentship MR/K016903 (RB).

ACKNOWLEDGMENTS

We would like to thank Dr. Helfrid Hochegger and Professor Marcos Malumbres and Dr. Mónica Álvarez-Fernández for their support and for donating reagents such as GWL, AAK and xlCdk1 mammalian expression constructs and primary MEFs containing loxP sites flanking exon 4 of the murine GWL gene, respectively. We would also like to acknowledge LifeArc (Formerly MRC Technology) for contributing funding towards to the PhD position of PJM, Dr. Antony Oliver for assisting with *in silico* and bioinformatics approaches to identify GWL *sogg* mutations and Professor Simon E. Ward for granting us access to the synthetic chemistry resources of the Sussex Drug Discovery Centre.

References

[1] Manning, G., Whyte, D. B., Martinez, R., Hunter, T., and Sudarsanam, S. (2002) The Protein Kinase Complement

of the Human Genome, *Science 298*, 1912 - 1934.

[2] Elphick, L. M., Lee, S. E., Gouverneur, V., and Mann, D. J. (2007) Using Chemical Genetics and ATP Analogues

To Dissect Protein Kinase Function, *ACS Chem Biol 2*, 299 - 314.

[3] Apsel, B., Blair, J. A., Gonzalez, B., Nazif, T. M., Feldman, M. E., Aizenstein, B., Hoffman, R., Williams, R. L., Shokat, K. M., and Knight, Z. A. (2008) Targeted polypharmacology: discovery of dual inhibitors of tyrosine and phosphoinositide kinases, *Nat Chem Biol 4*, 691-699.

[4] Barouch-Bentov, R., and Sauer, K. (2011) Mechanisms of drug resistance in kinases, *Expert Opin Investig Drugs 20*, 153-208.

[5] Fedorov, O., Muller, S., and Knapp, S. (2010) The (un)targeted cancer kinome, *Nat Chem Biol 6*, 166-169.

[6] Bishop, A. C., Ubersax, J. A., Petsch, D. T., Matheos, D. P., Gray, N. S., Blethrow, J., Shimizu, E., Tsien, J. Z., Schultz, P. G., Rose, M. D., Wood, J. L., Morgan, D. O., and Shokat, K. M. (2000) A chemical switch for inhibitorsensitive

alleles of any protein kinase, *Nature 407*, 395 - 401.

[7] Lopez, M. S., Choy, J. W., Peters, U., Sos, M. L., Morgan, D. O., and Shokat, K. M. (2013) Staurosporine-derived inhibitors broaden the scope of analog-sensitive kinase technology, *J Am Chem Soc 135*, 18153-18159.

[8] Zhang, C., Lopez, M. S., Dar, A. C., Ladow, E., Finkbeiner, S., Yun, C. H., Eck, M. J., and Shokat, K. M. (2013) Structure-guided inhibitor design expands the scope of analog-sensitive kinase technology, *ACS Chem Biol 8*, 1931-1938.

[9] Garske, A. L., Peters, U., Cortesi, A. T., Perez, J. L., and Shokat, K. M. (2011) Chemical genetic strategy for targeting protein kinases based on covalent complementarity, *Proc Natl Acad Sci U S A 108*, 15046-15052.

[10] Zhang, C., Kenski, D. M., Paulson, J. L., Bonshtien, A., Sessa, G., Cross, J. V., Templeton, D. J., and Shokat, K. M. (2005) A second-site suppressor strategy for chemical genetic analysis of diverse protein kinases, *Nat Methods 2*, 435-441.

[11] Bishop, A., Buzko, O., Heyeck-Dumas, S., Jung, I., Kraybill, B., Liu, Y., Shah, K., Ulrich, S., Witucki, L., Yang, F., Zhang, C., and Shokat, K. M. (2000) UNNATURAL LIGANDS FOR ENGINEERED

PROTEINS: New Tools for Chemical Genetics, *Annu. Rev. Biophys. Biomol. Struct. 29*, 577 - 606.

[12] Koch, A., Rode, H. B., Richters, A., Rauh, D., and Hauf, S. (2012) A chemical genetic approach for covalent inhibition of analogue-sensitive aurora kinase, *ACS Chem Biol 7*, 723-731.

[13] Kung, A., Schimpl, M., Ekanayake, A., Chen, Y. C., Overman, R., and Zhang, C. (2017) A Chemical-Genetic Approach to Generate Selective Covalent Inhibitors of Protein Kinases, *ACS Chem Biol 12*, 1499-1503.

[14] Kung, A., Chen, Y. C., Schimpl, M., Ni, F., Zhu, J., Turner, M., Molina, H., Overman, R., and Zhang, C. (2016) Development of Specific, Irreversible Inhibitors for a Receptor Tyrosine Kinase EphB3, *J Am Chem Soc 138*, 10554-10560.

[15] Blair, J. A., Rauh, D., Kung, C., Yun, C. H., Fan, Q. W., Rode, H., Zhang, C., Eck, M. J., Weiss, W. A., and Shokat, K. M. (2007) Structure-guided development of affinity probes for tyrosine kinases using chemical genetics, *Nat Chem Biol 3*, 229-238.

[16] Serafimova, I. M., Pufall, M. A., Krishnan, S., Duda, K., Cohen, M. S., Maglathlin, R. L., McFarland, J. M., Miller, R. M., Frodin, M., and Taunton, J. (2012) Reversible targeting of noncatalytic cysteines with chemically tuned electrophiles, *Nat Chem Biol 8*, 471-476.
[17] Gushwa, N. N., Kang, S., Chen, J., and Taunton, J. (2012) Selective Targeting of Distinct Active Site Nucleophiles by

Irreversible Src-Family Kinase Inhibitors, *J Am Chem Soc 134*, 20214 − 20217.
[18] Cohen, M. S., Zhang, C., Shokat, K. M., and Taunton, J. (2005) Structural Bioinformatics-Based Design of Selective, Irreversible Kinase Inhibitors, *Science 308*, 1318 - 1321.
[19] Liu, Y., and Gray, N. S. (2006) Rational design of inhibitors that bind to inactive kinase conformations, *Nat Chem Biol 2*, 358-364.
[20] Ocasio, C. A., Rajasekaran, M. B., Walker, S., Le Grand, D., Spencer, J., Pearl, F. M. G., Ward, S. E., Savic, V., Pearl, L. H., Hochegger, H., and Oliver, A. W. (2016) A first generation inhibitor of human Greatwall kinase, enabled

by structural and functional characterisation of a minimal kinase

domain construct, *Oncotarget 7*, 71182 - 71197.
[21] Wang, L., Luong, V. Q., Giannini, P. J., and Peng, A. (2014) Mastl kinase, a promising therapeutic target, promotes cancer

recurrence, *Oncotarget 5*, 11479 - 11489.
[22] Mochida, S., Maslen, S. L., Skehel, M., and Hunt, T. (2010) Greatwall phosphorylates an inhibitor of protein phosphatase 2A that is essential for mitosis, *Science 330*, 1670-1673.
[23] Burgess, A., Vigneron, S., Brioudes, E., Labbe, J. C., Lorca, T., and Castro, A. (2010) Loss of human Greatwall results in G2 arrest and multiple mitotic defects due to deregulation of the cyclin B-Cdc2/PP2A balance, *Proc Natl Acad Sci U S A 107*, 12564-12569.
[24] Grant, B. D., Hemmer, W., Tsigelny, I., Adams, J. A., and Taylor, S. S. (1998) Kinetic Analyses of Mutations in the Glycine-Rich Loop of cAMP-Dependent, *Biochemistry 37*, 7708 - 7715.
[25] Dar, A. C., Das, T. K., Shokat, K. M., and Cagan, R. L. (2012) Chemical genetic discovery of targets and anti-targets for cancer polypharmacology, *Nature 486*, 80-84.
[26] Tolstoluzhsky, N., Nikolaienko, P., Gorobets, N., Van der Eycken, E. V., and Kolos, N. (2013) Efficient Synthesis of Uracil-Derived Hexa- and Tetrahydropyrido[2,3-d]pyrimidines, *European Journal of Organic Chemistry 2013*, 5364-5369.
[27] Dar, A. C., and Shokat, K. M. (2011) The evolution of protein kinase inhibitors from antagonists to agonists of cellular signaling, *Annu Rev Biochem 80*, 769-795.
[28] Hari, S. B., Merritt, E. A., and Maly, D. J. (2013) Sequence determinants of a specific inactive protein kinase conformation, *Chem Biol 20*, 806-815.
[29] Alvarez-Fernandez, M., Sanchez-Martinez, R., Sanz-Castillo, B., Gan, P. P., Sanz-Flores, M., Trakala, M., Ruiz-Torres, M., Lorca, T., Castro, A., and Malumbres, M. (2013) Greatwall is essential to prevent mitotic collapse after nuclear envelope breakdown in mammals, *Proceedings of the National Academy of Sciences 110*, 17374-17379.
[30] Alexander, L. T., Mobitz, H., Drueckes, P., Savitsky, P., Fedorov, O., Elkins, J. M., Deane, C. M., Cowan-Jacob, S. W., and Knapp, S. (2015) Type II Inhibitors Targeting CDK2, *ACS Chem Biol 10*, 2116-2125.
[31] Burgess, S. G., and Bayliss, R. (2015) The structure of C290A:C393A Aurora A provides structural insights into kinase regulation, *Acta Crystallogr F Struct Biol Commun 71*, 315-319.
[32] Hegarat, N., Smith, E., Nayak, G., Takeda, S., Eyers, P. A., and Hochegger, H. (2011) Aurora A and Aurora B jointly coordinate chromosome segregation and anaphase microtubule dynamics, *J Cell Biol 195*, 1103-1113.

Supporting Information

Type II kinase inhibitors targeting the Cys-gatekeeper display orthogonality with wild type and Ala/Gly-gatekeeper kinases

Cory A. Ocasio*[a,f+], Alexander A. Warkentin[b+], Patrick J. McIntyre[c], Krister J. Barkovich[b], Clare Vesely[a], John Spencer[d], Kevan M. Shokat[b] and Richard Bayliss[e]

[a] Dr. Cory A. Ocasio*[+], Dr. Clare Vesely
Genome Damage and Stability Centre, School of Life Sciences, University of Sussex, Falmer, Brighton, BN1 9RQ (UK)
[b] Dr. Alexander A. Warkentin[+], Krister J. Barkovich, MD, Professor Kevan M. Shokat
Howard Hughes Medical Institute and Department of Cellular and Molecular Pharmacology, University of California, San Francisco, 600 16th Street, San Francisco, CA, 94158-2280 (US)
[c] Dr. Patrick J. McIntyre
Department of Molecular and Cell Biology, Henry Wellcome Building, University of Leicester, Leicester, LE1 9HN, (UK)
[d] Professor John Spencer
Department of Chemistry, School of Life Sciences, University of Sussex, Falmer, Brighton, BN1 9QJ (UK)
[e] Professor Richard Bayliss
School of Molecular and Cellular Biology, Faculty of Biological Sciences, University of Leeds, Leeds, LS2 9JT (UK)
[f] Current Address: The Francis Crick Institute, London, NW1 1AT (UK)
[+] Denotes joint first authors
[*] Correspondence: Cory A. Ocasio; tony.ocasio@crick.ac.uk

TABLE OF CONTENTS **Page**

Supplementary Figures

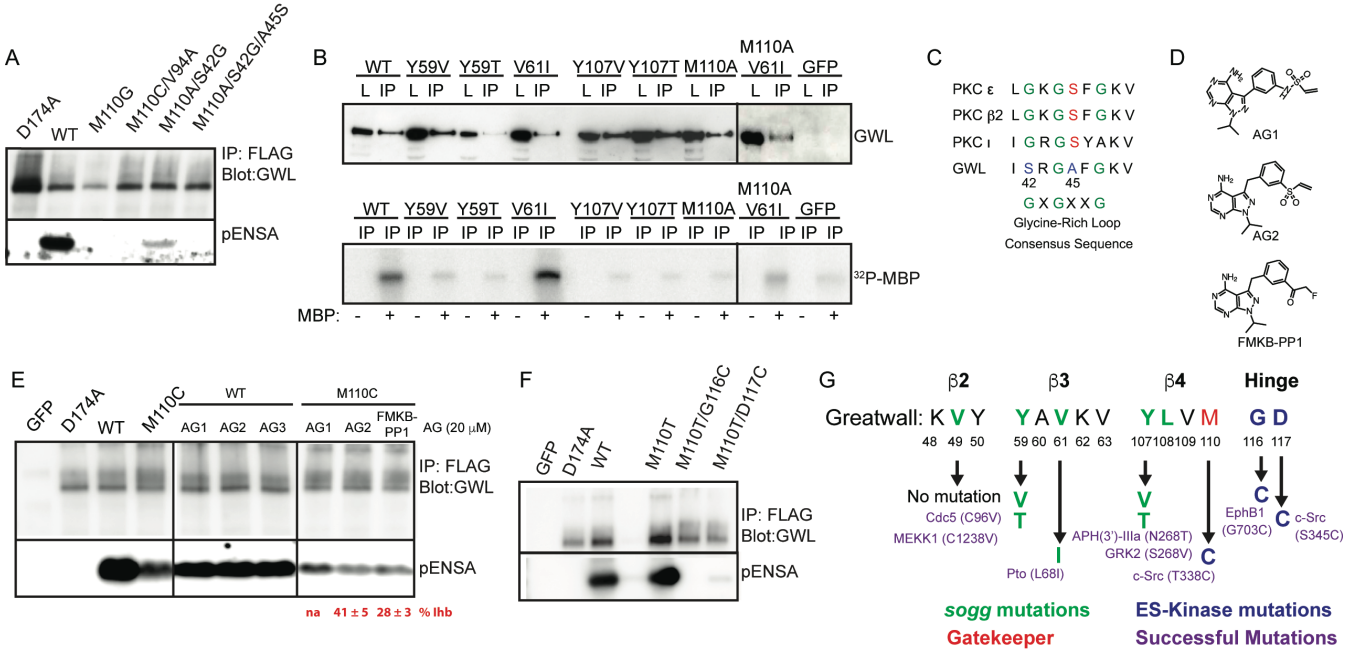

Figure S1. Attempts to identify rescuing *sogg* mutations and establish an ES-kinase system for Greatwall kinase. A) FLAG-tagged GWL or mutants D174A, M110G and the double and triple mutants M110C/V94A, M110A/S42G and M110A/S42G/A45S were expressed in human HEK 293T cells, immunoprecipitated and taken into kinase assays using ENSA as substrate. **B**) FLAG-tagged GWL or mutants Y59V, Y59T, V61I, Y106V, Y107T, M110A and double mutant M110A/V61I were expressed in human HEK 293T cells, immunoprecipitated and taken into kinase assays using myelin basic protein as substrate. **C**) Alignment of the glycine-rich loop region of GWL with those of other AGC kinases such as PKC isoforms ε, β2 and ι reveals incongruous amino acids at positions S42 and A45 of GWL. **D,E**) Analogue-sensitive, electrophilic kinase inhibitors **AG1-3** (**D**) were tested against immunoprecipitated WT and M110C GWL (**E**) in kinase assays using ESNA as substrate. **F**) FLAG-tagged GWL or mutants D174A, M110T and double mutants M110T/G116C and M110T/D117C were expressed in human HEK 293T cells, immunoprecipitated and taken into kinase assays using ENSA as substrate. **G**) Diagram illustrating *sogg* mutations made within β-sheets 2 – 4 and mutations of the gatekeeper position and select hinge region amino acids to cysteine. Mutations Y59V and Y59T were rationally incorporated particularly due to the stabilising effect of β-branched amino acids on β-sheets.

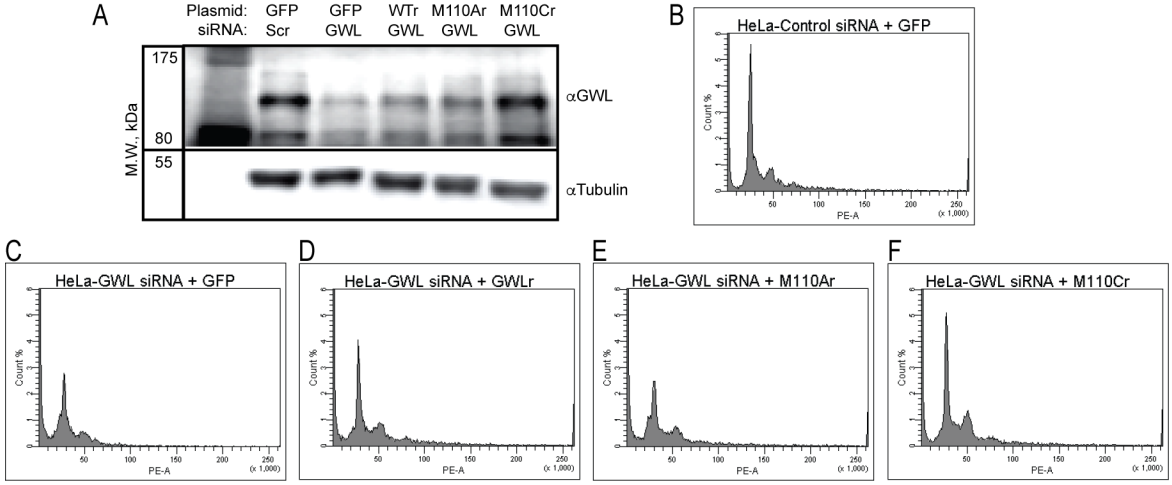

Figure S2. Cell cycle analysis of HeLa cells expressing siRNA-resistant GWL constructs. A) Rescue of RNAi-mediated GWL depletion by co-expression with siRNA-resistant WT (GWL)-, M110A- and MC-GWL constructs (GWLr = WT, M110Ar and M110Cr). **B-F**) FACS-cell cycle analysis of HeLa cells.

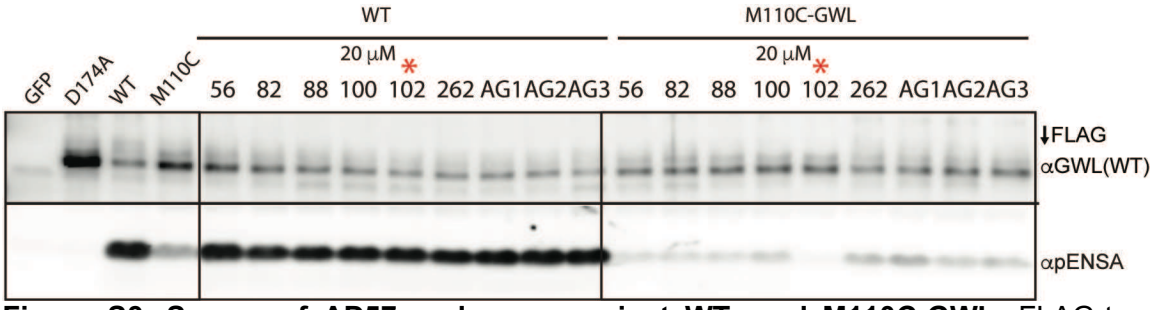

Figure S3. Screen of AD57-analogues against WT- and M110C-GWL. FLAG-tagged GWL and M110C mutant were expressed in human HEK293T cells, immunoprecipitated and taken into kinase assays in the presence of 20 μM concentrations of AD57-analogues 56, 82, 88, 100, 102 (ASDO1), 262 and AG1-2 and FMKB-PP1 (AG3) using ENSA as substrate.

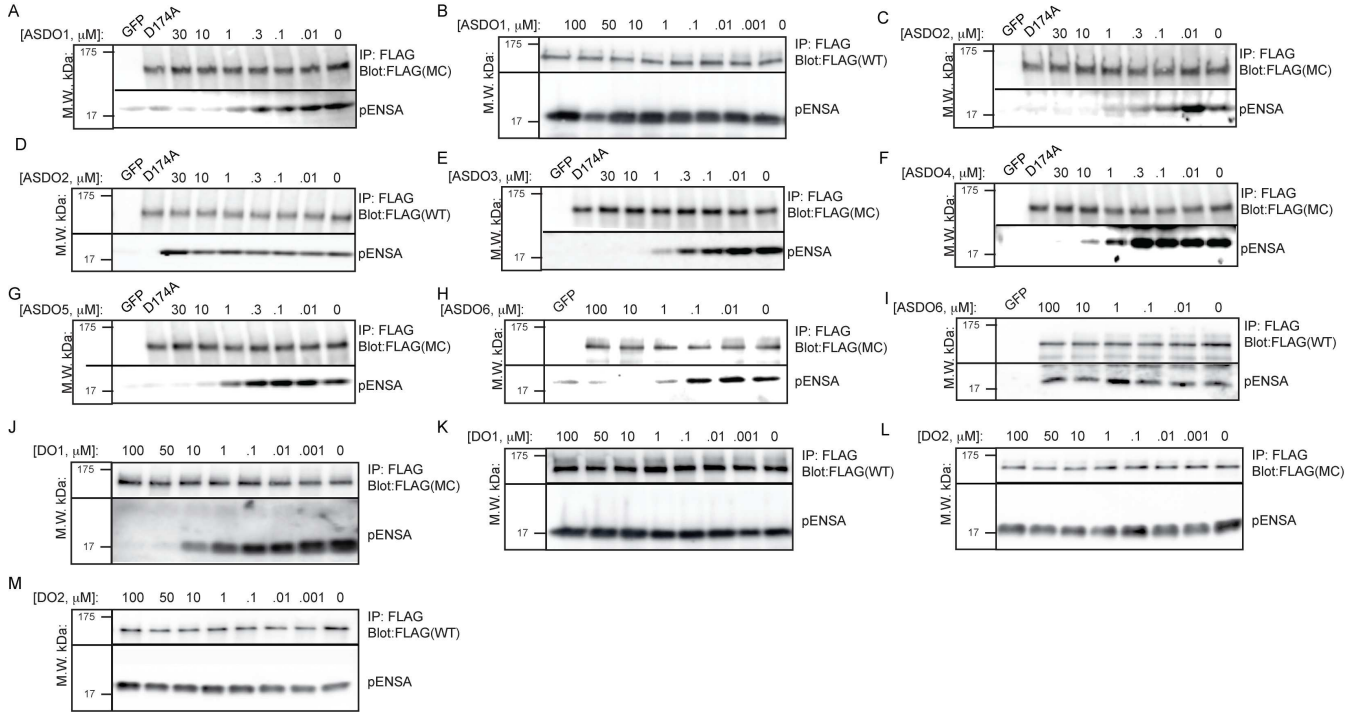

Figure S4. *In vitro* analysis of ASDO analogues by IP kinase assay and western analysis. A-M) FLAG-tagged GWL and M110C mutant were expressed in human HEK 293T cells, immunoprecipitated and taken into kinase assays in the presence of increasing concentrations of ASDO analogues and **DO1** and DO2 using ENSA as substrate.

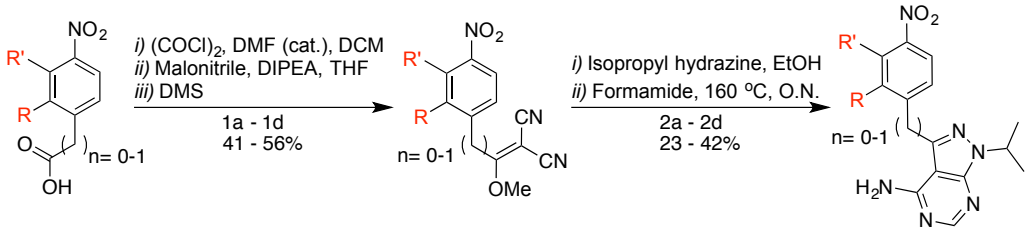

Supplemental Scheme 1. Synthetic route for nitrophenyl (or nitrophenylmethyl) pyrazolopyrimidine intermediates.

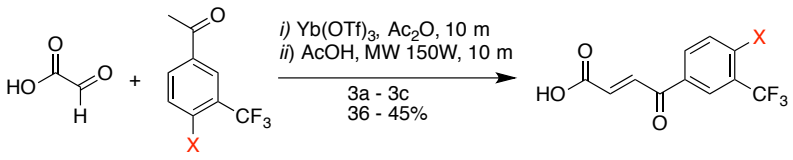

Supplemental Scheme 2. Synthetic route for 3-benzoylacrylic acids.

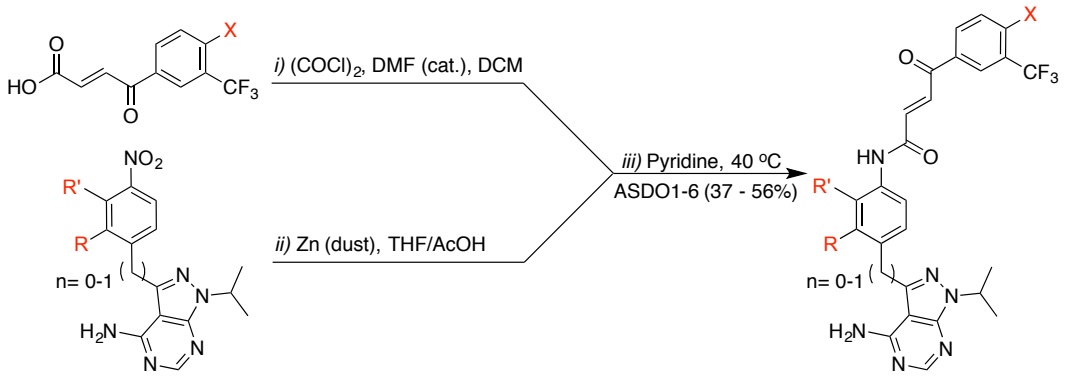

Supplemental Scheme 3. Synthesis of **ASDO1-6** by coupling of pyrazolopyrimidines with 3-benzoylacrylic acids.

A

Plate Barcode D6745PM	ASDO2 (1 μM) % Activity Remaining	% Inhibition	SD
Src	5	95	0
RIPK2	6	94	2
Lck	8	92	1
TrkA	9	91	2
Aurora B	11	89	0
HIPK2	19	81	2
MLK3	24	76	2
HER4	26	74	3
MKK1	27	73	2
VEG-FR	27	73	2
TAK1	30	70	9
IRAK4	30	70	1
CHK2	32	68	4
S6K1	36	64	6
CAMK1	40	60	21
CK1δ	51	49	1
ROCK 2	55	45	7
MST2	55	45	4
RSK1	62	38	6
BTK	63	37	15
GSK3b	67	33	14
MSK1	70	30	0
PAK4	70	30	6
PLK1	71	29	0
PKD1	73	27	1
PDK1	74	26	26
PKCa	74	26	14
JAK2	75	25	3
AMPK (hum)	75	25	2
EPH-A2	76	24	13
LKB1	76	24	6
TTK	79	21	3
DYRK1A	80	20	5
MARK3	80	20	1
SGK1	81	19	3
IGF-1R	82	18	9
CAMKKb	87	13	3
PRK2	87	13	4
SRPK1	88	12	2
PKA	91	9	1
PKBa	92	8	9
SYK	94	6	4
p38a MAPK	94	6	8
CK2	98	2	9
TBK1	99	1	14
JNK1	101	-1	4
PIM1	102	-2	3
EF2K	108	-8	8
NEK6	111	-11	2
SmMLCK	120	-20	3

B

Plate Barcode D6769PM	ASDO6 (1uM) % activity	% Inhibition	SD
SRPK1	16	84	1
RIPK2	27	73	1
MLK3	32	68	5
Src	38	62	1
VEG-FR	51	49	10
Lck	60	40	13
HER4	63	37	1
TrkA	65	35	6
ROCK 2	69	31	4
AMPK (hum)	70	30	4
TTK	70	30	3
PKD1	71	29	0
BTK	73	27	4
MKK1	73	27	4
MST2	77	23	4
PKCa	78	22	4
TAK1	78	22	7
DYRK1A	80	20	7
CHK2	82	18	0
PDK1	85	15	8
p38a MAPK	87	13	2
CAMK1	88	12	1
RSK1	91	9	3
SGK1	91	9	4
PIM1	92	8	9
CAMKKb	94	6	3
JAK3	94	6	10
GSK3b	95	5	7
MSK1	95	5	3
S6K1	95	5	3
TBK1	96	4	8
CK1δ	96	4	6
JNK1	96	4	0
EPH-A2	97	3	31
PKA	97	3	4
PKBa	97	3	2
EF2K	98	2	11
PAK4	98	2	3
PRK2	99	1	0
SYK	99	1	5
IRAK4	100	0	9
SmMLCK	101	-1	3
HIPK2	102	-2	13
PLK1	103	-3	5
CK2	104	-4	3
LKB1	104	-4	15
MARK3	106	-6	16
NEK6	123	-23	2
IGF-1R	142	-42	13

Figure S5. Kinase Profiling Express Screen. ASDO2 (**A**) and **ASDO6** (**B**) were tested against 50 select kinases at a concentration of 1 μM. The Kinase Profiling Express Screen was conducted at the International Centre for Kinase Profiling, University of Dundee.

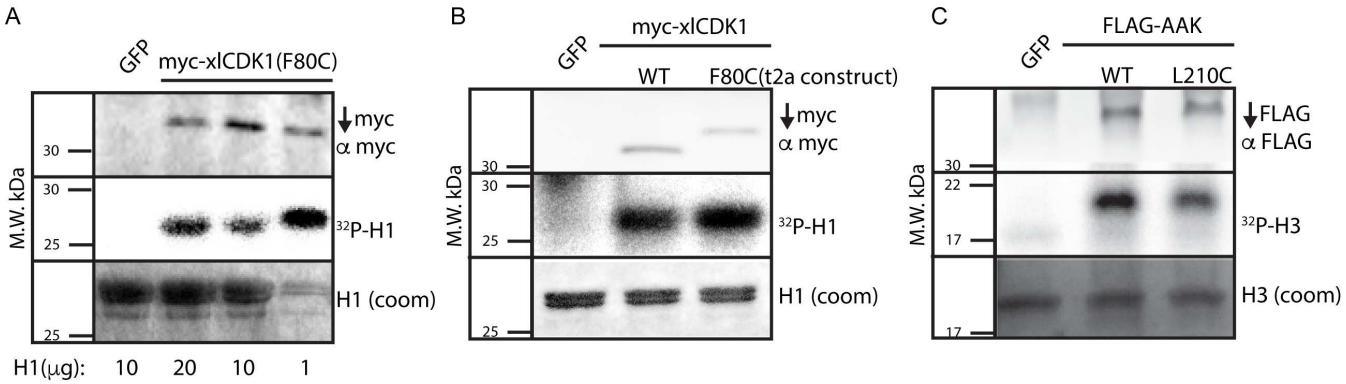

Figure S6. xICDK1 and Aurora A kinase assays. A) In order to establish an xICDK1 kinase assay, MYC-tagged xICDK1 and F80C mutant were expressed in HEK293T cells, immunoprecipitated with 4 μg of anti-MYC antibody and 5 μL Protein G magnetic Dynabeads and taken into radioactive ^{32}P-ATP kinase assays with increasing amounts of the substrate histone H1. **B**) After optimisation of the xICDK1 kinase assay, WT and F80C mutant xICDK1 were assayed again to establish the relative activity of the mutant vs. WT kinase, revealing the mutant was significantly more active than WT. **C**) FLAG-tagged WT and L210C Aurora A kinase (AAK) were expressed in HEK293T cells, immunoprecipitated and taken into radioactive ^{32}P-ATP kinase assays using histone H3 as substrate. L210C-AAK demonstrated significant activity compared to GFP expressing cells, but slightly less activity than WT AAK.

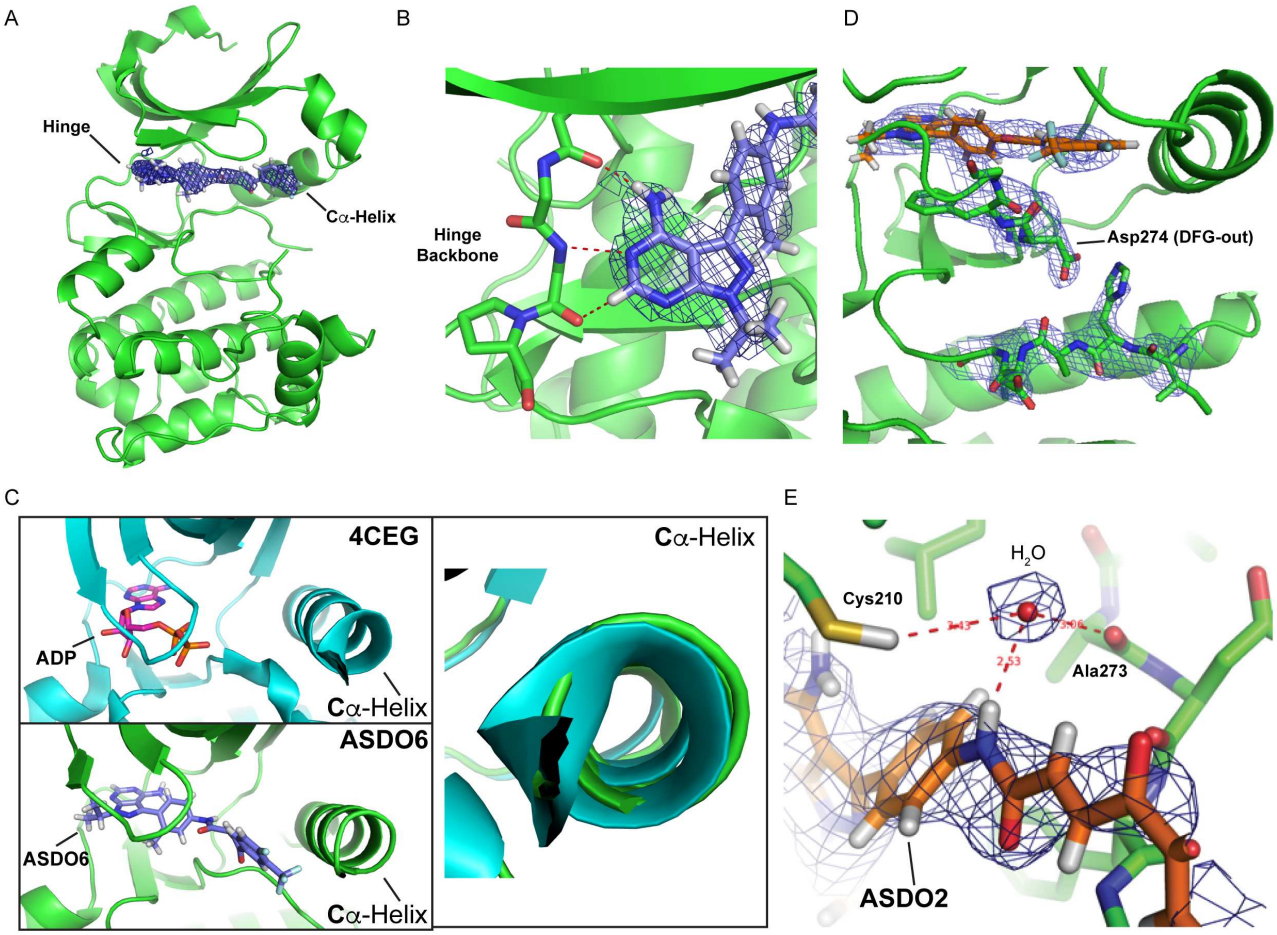

Figure S7. X-ray co-crystal structures of ASDO6 and ASDO2 help reveal the molecular level basis for cysteine-gatekeeper specificity. A) The final 2mFo-DFc electron density map is shown as a mesh contoured at 1 σ with **ASDO6** bound to the ATP-binding pocket and stretching from the hinge to the Cα-helix. **B**) **ASDO6** makes the expected interactions with the hinge region of Aurora-A kinase, typical of an ATP-competitive inhibitor. P-loop has been removed for clarity. **C**) Front view (left panels) of compound **ASDO6** (purple) and ADP (pink) showing the Cα-helix and end view (right panel) of the Cα-helix in **ASDO6** structure (green) and ADP structure (cyan, PDB: 4CEG). **D**) **ASDO2**-bound Aurora A kinase is in the DFG-out conformation as expected with a type II inhibitor. Compound is bound adjacent to Cα-

helix, distorting it. **E**) Water-mediated hydrogen bonds between **ASDO2**, the carbonyl of Ala273 and the side-chain of Cys210.

Supplementary Methods

Antibodies and Western Analysis

Mouse monoclonal anti-FLAG® M2 and rabbit anti-MASTL (GWL, Prestige Antibodies) antibodies were purchased from Sigma-Aldrich and polyclonal rabbit anti-phospho(Ser67)-ENSA/ARPP19 and anti-ENSA antibodies were purchased from Cell Signaling Technology. Mouse monoclonal anti-c-Myc (9E10) and mouse and rabbit derived antibodies for loading controls α-tubulin (DM1A) and GAPDH respectively were purchased from Abcam. Secondary antibodies were HRP-conjugated, polyclonal goat-derived antibodies against mouse and rabbit (Dako, Agilent Technologies). Western blot analysis of GWL, ENSA, phospho-ENSA, and the loading controls α-tubulin and GAPDH was accomplished through SDS-PAGE of cell lysates in 1X SDS-loading buffer containing β-mercaptoethanol (5X buffer: 0.25 % w/v Bromophenol blue, 0.5 M DTT, 50% v/v glycerol, 10% v/v SDS (sodium dodecyl sulphate) and 0.25M Tris-HCl pH 6.8) and transfer of protein onto PVDF using the Trans-Blot Turbo System (Bio-Rad). Quantitation of western blot protein intensity was performed by densitometry using ImageJ and data were plotted using Prism 6.0.

Expression Constructs

The mammalian expression construct for N-terminally FLAG-tagged full-length human GWL and Aurora A kinase have previously been described[30-31]. The plasmid for expression of *Xenopus laevis* MYC-Cdk1 was a kind gift from Helfrid Hochegger. Recombinant His-tagged ENSA was purified using Ni-NTA agarose (QIAGEN) from BL21 *E. coli* following the manufacturer's recommended protocol. FLAG-GWL (WT or M110C) was cloned into the pLVX-IRES-Puro (Clontech) lentiviral vector through restriction digestion of the FLAG-GWL construct with NotI and ligation of this product with NotI digested and phosphatase (CIP) treated pLVX-IRES-Puro plasmid. Ligation with T4 DNA Ligase (NEB) proceeded at 15 °C overnight after which 2 ul was transformed into supercompetent DH5□. After plating and growing transformants overnight, colonies were selected, amplified in the presence of ampicillin and then harvested to prepare DNA minipreps. Miniprepped DNA was digested with BamHI and analysed by agarose gel electrophoresis to confirm that GWL expressing pLVX clones contained properly oriented inserts. Clones were then amplified and used to prepare lentiviral particles according to the instructions in the Lenti-X™ Lentiviral Expression System Manual (Clontech).

Mutagenesis

All mutagenesis reactions were carried out using the QuikChange II Site-Directed or Lightning Multi Site-Directed Mutagenesis Kits (Agilent) according to the manufacturer's instructions. All plasmids

were sent to GATC Biotech for Sanger sequencing to confirm the mutations. Mutagenic primers were purchased from Eurofins and are listed below.

GWL

Y59V:	F – GAA AGG CGG CAA ATT GGT TGC AGT AAA GGT TG,
	R – CAA CCT TTA CTG CAA CCA ATT TGC CGC CTT TC
Y59T:	F – GAA AGG CGG CAA ATT GAC TGC AGT AAA GGT TG,
	R – CAA CCT TTA CTG CAG TCA ATT TGC CGC CTT TC
V61I:	F – GGC AGA AAG GCG GCA AAT TGT ATG CAA TAA AGG TTG,
	R – CAA CCT TTA TTG CAT ACA ATT TGC CGC CTT TCT GCC
Y107V:	F – GCA GTC TGC AAA CAA TGT CGT CTT GGT AAT GG,
	R – CCA TTA CCA AGA CGA CAT TGT TTG CAG ACT GC
Y107T:	F – GCA GTC TGC AAA CAA TGT CAC CTT GGT AAT GG,
	R – CCA TTA CCA AGG TGA CAT TGT TTG CAG ACT GC
D174A:	F – GGGTCATATTAAACTGACGGCTTTTGGCCTTTCAAAAGTTAC,
	R – GTAACTTTTGAAAGGCCAAAAGCCGTCAGTTTAATATGACCC
M110V:	F – CAATGTCTACTTGGTAGTGGAATATCTTATTGGGG,
	R – CCCCAATAAGATATTCCACTACCAAGTAGACATTG
M110T:	F – GTCTACTTGGTAACGGAATATCTTATTGGGGG,
	R – CCCCCAATAAGATATTCCGTTACCAAGTAGAC
M110C:	F – GTCTACTTGGTATGCGAATATCTTATTGGG,
	R – CCCAATAAGATATTCGCATACCAAGTAGAC
M110S:	F – CAAACAATGTCTACTTGGTATCGGAATATCTTATTG,
	R – CAATAAGATATTCCGATACCAAGTAGACATTGTTTG
M110A:	F – CAATGTCTACTTGGTAGCGGAATATCTTATTGGGG,
	R – CCCCAATAAGATATTCCGCTACCAAGTAGACATTG
M110G:	F – CAATGTCTACTTGGTAGGGGAATATC,
	R – CAATAAGATATTCCCCTACCAAGTAGACATTGTTTG
V94A:	F – CATTCATTGCCCATTTGTATTATTCACTG,
	R – CAGTGAATAATACAAATGGGCAATGAATG
S42G:	F – CATAGTGAAGCCCATTGGCCGGGGCGCCTTCG,
	R – CGAAGGCGCCCCGGCCAATGGGCTTCACTATG
A45S:	F – CATTGGCCGGGGCTCCTTCGGGAAAG,
(with S42G)	R – CTTTCCCGAAGGAGCCCCGGCCAATG
G116C:	F – CTTATTGGGTGTGATGTCAAG,
	R – CTTGACATCACACCCAATAAG
G117C:	F – CTTATTGGGGGATGTGTCAAGTCTC,
	R – GAGACTTGACACATCCCCCAATAAG

siRNA_ resistant GWL mutations (Figure S1):

F – CAAAAGGACACTACTCCTTACTCTTCAAAACTCCTAAAATCATG

R – CATGATTTTAGGAGTTTTGAAGAGTAAGGAGTAGTGTCCTTTTG

Aurora-A Kinase

L210C: F – GTCTACCTAATTTGCGAATATGCACC,

R – GGTGCATATTCGCAAATTAGGTAGAC

xlCDK1

F80C: F – CAAGGTTGTATCTTATCTGTGAGTTTCTCTCCATGG,

R – CCATGGAGAGAAACTCACAGATAAGATACAACCTTG

Cell Culture, Compound Preparation and FACS analysis

MEFs and HEK 293T cells were cultured in Dulbecco's modified Eagle Medium (DMEM) supplemented with 10% v/v FCS, 2 mM L-glutamine, 100 U/ml penicillin and 0.1 mg/ml streptomycin in a 37 °C, 5% CO_2 incubator. For GWL depletion, 10 ul of AdCre (Vector Biolabs) was added to a 10 cm dish of MEFs in culture. After 3 d, cells were then treated with 500 ul of GWL expressing lentivirus (0.45 micron filtered). Synthetically derived ASDO compounds, 4-(4-ethoxy-phenyl)-4-oxo-but-2-enoic acid (4-ethyl-phenyl)-amide (DO2, Sigma-Aldrich/Merck), staurosporine (Cell Signalling Technology) and AD57 were dissolved in DMSO and stored at -20 °C in glass vials. Cells transfected with or without GWL targeting siRNA (HS_MASTL_6)[18] and Qiagen AllStars negative control were harvested, washed with PBS and fixed in 70% EtOH overnight at 4 °C. Next, cells were pelleted and washed with 1% BSA in PBS. After pelleting, cells were re-suspended and incubated with propidium iodide (PI) solution for at least 6 h or overnight (PI solution: 20 □g/ml PI, 0.1% Triton X-100, 200 □g ml^{-1} RNAse (all from Sigma) diluted in 0.5% BSA in PBS). Cell cycle analysis was performed on the BD Accuri™ C6 Plus personal flow cytometer and data analysed using FCS Express 6 flow cytometry software.

Proliferation Assays

MEF cells were seeded at a density of 1000 and 2000 cells/well, respectively, in clear 96-well plates and allowed to grow for 5 – 6 d in the presence of inhibitors or DMSO. After the indicated time-point, all cells were treated with CellTiter-Blue Reagent (Promega) and allowed to incubate at 37 °C for an additional 3 h. After 3 h, fluorescence was measured using the GloMax-Multi Detection System. All concentration-dependent cellular proliferation assays were performed 5 times with replicates ranging from 4 to 10 per point and quantitation of average normalized proliferation was reported as % of the DMSO control ± S.D. and plotted using Prism 6.0. The t-test statistical module of Prism 6.0 was used to determine p-values (ns (not statistically significant): $P \leq 0.01$; ***: $P \leq 0.001$; ****).

Chemical Synthesis

All commercial reagents were purchased from Sigma-Aldrich, Alfa Aesar, Combi-Blocks, TCI (UK) and Princeton Biomolecular and were of the highest available purity. Anhydrous solvents were purchased

from Acros (AcroSeal) or Sigma-Aldrich (SureSeal) and were stored under nitrogen. Proton nuclear magnetic resonance spectra were recorded at 500 or 400 MHz on a Varian VNMRS 500 MHz spectrometer, at 25 °C. Carbon Nuclear Magnetic Resonance spectra were recorded at 125 MHz on a Varian 500 MHz spectrometer. It should be noted that we did not detect C-F heteronuclear coupling due to CF_3 in the ^{13}C NMR mainly due to overlapping peaks. LCMS data were recorded on a Waters 2695 HPLC using a Waters 2487 UV detector and a Thermo LCQ ESI-MS. Samples were eluted through a Phenomenex Lunar 3µ C18 50 mm × 4.6 mm column, using water and acetonitrile acidified with 0.1% formic acid at 1 ml/min and detected at 254 nm. The gradient employed was a 4 or 7 min. method of 5-95% MeCN. High-resolution Mass Spectra (HRMS) were recorded at the University of Sussex Mass Spectrometry Centre on a high-resolution Orbitrap-XL instrument (Thermofisher). All experiments were carried out under an inert atmosphere of N_2 unless otherwise stated.

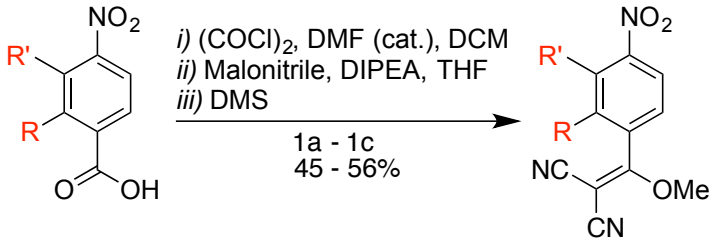

Intermediate	R	R'	%
1a	H	H	46
1b			45
1c	Me	H	56

General procedure for the synthesis of 2-[methoxy(4-nitrophenyl)methylidene]propanedinitriles (**1a** – **1c**)[1]. 2-[Methoxy(4-nitrophenyl)methylidene]propanedinitrile (**1a**) was prepared by slowly adding a 2.0 M solution of oxalyl chloride in DCM (0.30 mL, 3.52 mmol, 1.2 eq.) to a solution of benzoic acid (0.49 g, 2.93 mmol, 1.0 eq.) in 15 mL DCM containing 1 drop of DMF at RT for 30 min. This solution was then concentrated *in vacuo* and then re-dissolved in 5 ml of THF containing malonitrile (0.23 g, 3.52 mmol, 1.2 eq.) This mixture was cooled to 0 °C before drop-wise addition of DIPEA (1.28 mL, 7.33 mmol, 2.5 eq.). This reaction was allowed to warm to room temperature before being mixed for an additional 2 h. Next, dimethyl sulfate (DMS, 0.33 mL, 3.52 mmol, 1.2 eq.) was added, after which the temperature was increased to 70 °C. This was allowed to react for 4 h before bringing the temperature down to RT. At this stage, the reaction proceeded overnight before being worked-up with 1 N HCl (aq.) and extracted with ethyl acetate. Extracts were washed with water and brine and then dried with $MgSO_4$. The crude mixture was purified by silica chromatography using a hexanes/ethyl acetate solvent system (ethyl acetate gradient increased over time from 0 – 60%). Concentration of the extract yielded 0.31 g (1.37 mmol, 46%) of a yellow, oily material. ^1H NMR (500 MHz, Chloroform-*d*) δ 7.99 (d, *J* = 6.5 Hz, 2H), 7.24 (d, *J* = 6.5 Hz, 2H), 4.01 (s, 3H). ^{13}C NMR (126 MHz, $CDCl_3$) δ 183.8, 161.7, 132.6, 126.9, 125.8, 110.0, 49.8.

2-[Methoxy(4-nitronaphthalen-1-yl)methylidene]propanedinitrile (**1b**) was made according to the general procedure reported for **1a**. ^1H NMR (500 MHz, Chloroform-*d*) δ 8.54 (d, *J* = 8.2 Hz, 1H), 8.25 (d, *J* = 7.8 Hz, 1H), 7.94 – 7.82 (m, 3H), 7.72 (d, *J* = 7.8 Hz, 1H), 3.76 (s, 3H). ^{13}C NMR (126 MHz, $CDCl_3$) δ 182.3, 149.6, 130.8, 130.7, 130.7, 130.2, 126.8, 125.0, 124.2, 123.8, 122.2, 111.7, 110.4, 60.3.

2-[Methoxy(2-methyl-4-nitrophenyl)methylidene]propanedinitrile (**1c**) was made according to the general procedure reported for **1a**. ^{1}H NMR (500 MHz, Chloroform-*d*) δ 8.11 (d, *J* = 6.7 Hz, 1H), 7.52 (m, 2H), 4.02 (s, 3H), 2.68 (s, 3H).

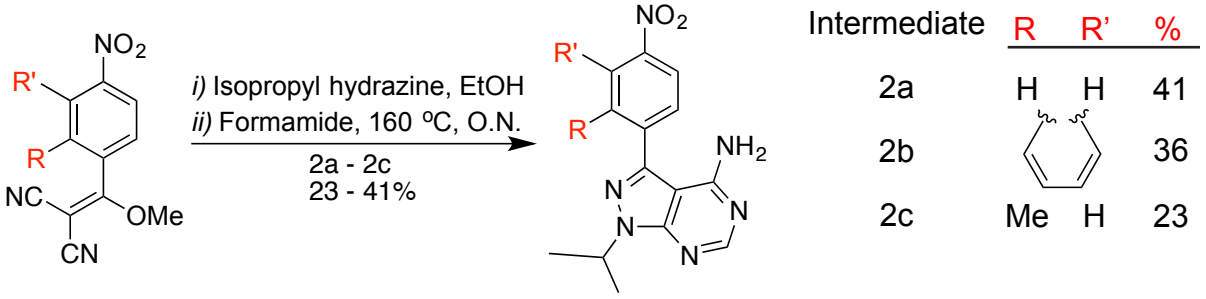

Intermediate	R	R'	%
2a	H	H	41
2b			36
2c	Me	H	23

General procedure for the synthesis of 3-(4-nitrophenyl)-1-(propan-2-yl)-1H-pyrazolo[3,4-d]pyrimidin-4-amines (**2a** – **2c**)[1]. 3-(4-Nitrophenyl)-1-(propan-2-yl)-1H-pyrazolo[3,4-d]pyrimidin-4-amine (**2a**) was prepared by mixing **1a** (0.31 g, 1.37 mmol, 1 eq.) with isopropyl hydrazine (0.12 g, 1.65 mmol, 1.2 eq.) and TEA (3.71 mL, 27.5 mmol, 20 eq.) in 5 mL of EtOH. After 1h, the reaction was concentrated and generation of the pyrazole was confirmed by LCMS-LCQ: 7 mins, 5-95% MeCN, Rt = 3.75 mins; $[M+H]^+$ calculated for $C_{13}H_{13}N_5O_2$ 272.11; found 272.17. The pyrazole was then diluted with 5 mL of formamide (0.3M **1a**) and left to reflux ON at 160 °C. After cooling, the reaction was diluted with 50 mL of ice cold water, which was then filtered over a pad of celite. Extracting the filtrate with ethyl acetate and concentrating the extracts gave 190 mg (0.64 mmol, 41%) of a yellow powder that was used in the next reaction without further purification. ^{1}H NMR (500 MHz, DMSO-d_6) δ 8.30 (d, *J* = 8.7 Hz, 1H), 8.21 (s, 1H), 7.89 (d, *J* = 8.5 Hz, 1H), 6.59 (s, 1H), 5.09 (hept, *J* = 6.7 Hz, 1H), 1.51 (d, *J* = 6.6 Hz, 3H). ^{13}C NMR (126 MHz, dmso) δ 158.3, 155.7, 147.6, 141.4, 140.2, 129.5, 124.3, 123.9, 110.0, 30.9, 22.0. LCMS-LCQ: 4 mins, 5-95% MeCN, Rt = 1.16 mins; $[M+H]^+$ calculated for $C_{14}H_{14}N_6O_2$ 299.30; found 299.17.

3-(4-Nitronaphthalen-1-yl)-1-(propan-2-yl)-1H-pyrazolo[3,4-d]pyrimidin-4-amine (**2b**) was made according to the general procedure reported for **2a**. After 1h of mixing **1d**, isopropyl hydrazine and TEA in ethanol, the reaction was concentrated and generation of the pyrazole was confirmed by LCMS-LCQ: 4 mins, 5-95% MeCN, Rt = 0.71 mins; $[M+H]^+$ calculated for $C_{17}H_{15}N_5O_2$ 322.12; found 321.98. ^{1}H NMR (500 MHz, DMSO-d_6) δ 8.44 (d, *J* = 8.7 Hz, 1H), 8.37 (d, *J* = 7.8 Hz, 1H), 8.28 (s, 1H), 8.04 (d, *J* = 8.4 Hz, 1H), 7.84 (t, 1H), 7.77 – 7.68 (m, 2H), 7.37 – 5.83 (s br, 2H), 5.14 (hept, *J* = 6.7 Hz, 1H), 1.53 (d, *J* = 6.7 Hz, 6H). ^{13}C NMR (126 MHz, dmso) δ 158.2, 156.2, 153.6, 147.2, 140.6, 137.1, 133.0, 129.9, 128.5, 127.8, 127.1, 125.4, 124.0, 122.9, 110.0, 49.0, 22.2. LCMS-LCQ: 4 mins, 5-95% MeCN, Rt = 0.74 mins; $[M+H]^+$ calculated for $C_{18}H_{16}N_6O_2$ 349.35; found 349.20.

3-(2-Methyl-4-nitrophenyl)-1-(propan-2-yl)-1H-pyrazolo[3,4-d]pyrimidin-4-amine (**2c**) was made according to the general procedure reported for **2a**. After 1h of mixing **1b**, isopropyl hydrazine and TEA in ethanol, the reaction was concentrated and generation of the pyrazole was confirmed by LCMS-LCQ:

4 mins, 5-95% MeCN, Rt = 3.07 mins; $[M+H]^+$ calculated for $C_{14}H_{15}N_5O_2$ 286.12; found 286.02. ^{1}H NMR (500 MHz, DMSO-d_6) δ 8.18 (s, 1H), 7.22 (s, 2H), 7.17 (d, J = 8.1 Hz, 1H), 6.73 (d, J = 8.2 Hz, 2H), 5.16 (s, 2H), 5.01 (hept, J = 6.7 Hz, 1H), 2.12 (s, 3H), 1.46 (d, J = 6.7 Hz, 6H). LCMS-LCQ: 4 mins, 5-95% MeCN, Rt = 2.13 mins; $[M+H]^+$ calculated for $C_{15}H_{16}N_6O_2$ 313.33; found 313.17.

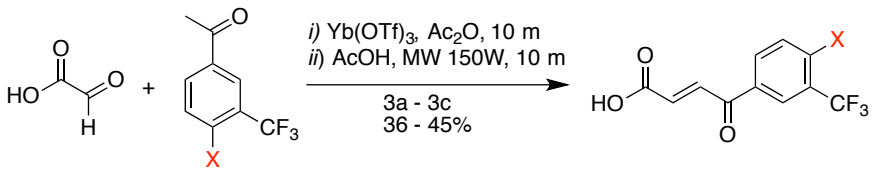

Intermediate	X	%
3a	H	39
3b	F	36
3c	Cl	45

General procedure for the synthesis of 3-benzoyl acrylic acids (**3a** – **3c**)[2]. To prepare (2E)-4-oxo-4-[3-(trifluoromethyl)phenyl]but-2-enoic acid (**3a**), glyoxylic acid monohydrate (2.2 g, 23.9 mmol), acetic anhydride (2.4 mL, 25.2 mmol) and ytterbium triflate (0.37 g, 0.59 mmol) were combined in a microwave reaction vial and stirred at room temperature for 10 min. Then, *m*-(trifluoromethyl)benzoylacetophenone (5 g, 24 mmol) and glacial acetic acid (4 mL) were added. The reaction vial was sealed, and the mixture was subjected to microwave irradiation for 10 min. at 150 W (< 6 bar internal pressure). After completion of the reaction, the dark brown/black mixture was diluted with water, basified with K_2CO_3 (25% aq.) and washed with DCM (5X 60 mL). Then, the aqueous phase was cooled in an ice-bath and acidified with HCl (concentrated aq.). The solid product was filtered off, washed with water and dried in air at 50 °C for 24 h to give 2.3 g (39%) of a light brown solid. ^{1}H NMR (500 MHz, DMSO-d_6) δ 13.06 (s, 1H), 8.33 (d, J = 7.8 Hz, 1H), 8.27 (s, 1H), 8.06 (d, J = 7.9 Hz, 1H), 7.92 (d, J = 15.7 Hz, 1H), 7.80 (t, J = 7.9 Hz, 1H), 6.71 (d, J = 15.5 Hz, 1H). ^{13}C NMR (126 MHz, $CDCl_3$) δ 194.0, 171.4, 142.2, 141.0, 138.9, 138.0, 135.7, 135.6, 135.3, 133.2, 109.9.

(2E)-4-[4-Fluoro-3-(trifluoromethyl)phenyl]-4-oxobut-2-enoic acid (**3b**) was made according to the general procedure reported for **3a**. ^{1}H NMR (500 MHz, DMSO-d_6) δ 13.17 (s, 1H), 8.43 (ddd, J = 8.1, 6.8 (H-F), 2.2 (H-F) Hz, 1H), 8.33 (dd, J = 6.8 (H-F), 2.0 (H-F) Hz, 1H), 7.92 (d, J = 15.6 Hz, 1H), 7.71 (t, J = 8.5, 6.8 (H-F) Hz, 1H), 6.71 (d, J = 15.6 Hz, 1H). ^{13}C NMR (126 MHz, dmso) δ 188.1, 166.6, 136.8, 136.7, 136.3, 136.1, 134.2, 128.6, 118.7, 118.5, 110.0.

(2E)-4-[4-Chloro-3-(trifluoromethyl)phenyl]-4-oxobut-2-enoic acid (**3c**) was made according to the general procedure reported for **3a.** ^{1}H NMR (500 MHz, DMSO-d_6) δ 13.06 (s, 1H), 8.33 – 8.31 (m, 2H), 7.93 (d, J = 8.8 Hz, 1H), 7.89 (d, J = 15.6 Hz, 1H), 6.72 (d, J = 15.5 Hz, 1H). ^{13}C NMR (126 MHz, $CDCl_3$) δ 193.2, 171.3, 140.8, 140.5, 139.5, 139.0, 139.0, 137.7, 134.5, 133.1, 110.0.

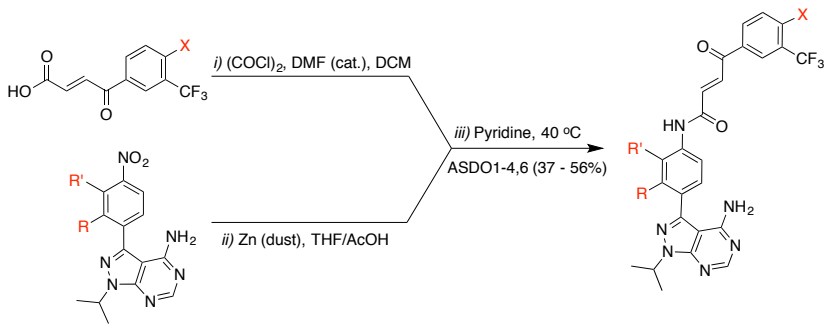

Intermediate	R	R'	X	%
ASDO1	H	H	H	41
ASDO2	H	H	F	43
ASDO3	H	H	Cl	56
ASDO4			H	37
ASDO6	Me	H	F	37

General procedure for the coupling of the 3-phenyl acrylic acids with 3-phenyl pyrazolopyrimidines (ASDO1-4 & 6). To a dry round bottom flask was added **2a** (20 mg, 0.067 mmol, 1.2 eq.) in 1 mL of AcOH/THF (1:1). Zn dust (13 mg, 0.20 mmol, 3.5 eq.) was added slowly and in portions over 5 mins. The reaction was mixed vigorously at 40 ºC over the next 3 h and monitored closely by TLC (DCM/ethyl acetate (1:1)). Next, the reaction was diluted in ethyl acetate, filtered over a pad of celite and washed with water thrice. This was then washed with brine, dried with magnesium sulfate and concentrated *in vacuo* to yield a brownish solid amine (deep purple colour with ninhydrin stain). This amine was diluted with 500 ul of pyridine and chilled on ice before being used as a coupling partner in the next step. In parallel to this reaction, the conversion of the acrylic acid to an acid chloride was effected by combining **3a** (13.7 mg, 0.057 mmol, 1 eq.) with oxalyl chloride $(COCl)_2$ (2M in DCM, 28.5 ul, 1 eq.) and 1 drop of DMF (catalytic). This solution was allowed to stir for 30 min. before removal of DCM by roto-evaporation; the resulting acid chloride was diluted with 200 ul of DMF. This acid chloride solution was then slowly added to a solution of the chilled amine solution. After 10 min., the reaction was allowed to warm to room temperature for 30 min. and then 40 ºC for 1 h. Finally, the reaction was diluted with ethyl acetate, washed with water and brine thrice, concentrated and purified by silica chromatography using a DCM/ethyl acetate solvent system (ethyl acetate gradient increased over time from 0 – 90%). To ensure that the remaining traces of the amine were removed, the resulting compound was purified further by preparatory TLC (Analtech Uniplates, Silica GF, 250 μM, 20 cm X 20 cm) under isocratic conditions using DCM/ethyl acetate (1:1). After etching off the correct band from the TLC plate, the silica was pulverised, mixed with ethyl acetate, filtered through a frit and the resulting filtrate was concentrated to yield 11.6 mg (0.023 mmol, 41%) of (2E)-N-{4-[4-amino-1-(propan-2-yl)-1H-pyrazolo[3,4-d]pyrimidin-3-yl]phenyl}-4-oxo-4-[3-(trifluoromethyl)phenyl]but-2-enamide (**ASDO1**). ^{1}H NMR (500 MHz, DMSO-d_6) δ 10.80 (s, 1H), 8.37 (d, *J* = 4.5 Hz, 1H), 8.29 (s, 1H), 8.21 (s, 1H), 7.97 (d, J = 4.5 Hz, 1H), 7.88 (d, J = 16 Hz, 1H), 7.83 (d, J = 12 Hz, 1H), 7.81 (t, J = 4.5 Hz, 1H), 7.64 (d, J = 12 Hz, 1H), 7.25 (d, J = 16 Hz, 1H), 6.74 (s, 2H), 5.04 (hept, J = 6.5 Hz, 1H), 1.45 (d, J = 6.5 Hz, 6H). ^{13}C NMR (126 MHz, $CDCl_3$) δ 188.2, 162.0, 157.2, 147.7, 144.3, 137.2, 136.5, 131.9, 131.9, 131.6, 131.6, 130.1, 130.1, 129.5, 129.7, 129.1, 125.6, 125.5, 120.9, 100.3, 49.7, 21.8. LCMS-LCQ: 7 mins, 5-95% MeCN, Rt = 3.64 mins, > 99% purity; $[M+H]^+$ calculated for $C_{25}H_{21}F_3N_6O_2$ 495.17; found 495.27. HRMS (ESI): $[M+H]^+$ calculated for $C_{25}H_{21}F_3N_6O_2$ 495.1678, found 495.1836.

(2E)-N-{4-[4-Amino-1-(propan-2-yl)-1H-pyrazolo[3,4-d]pyrimidin-3-yl]phenyl}-4-[4-fluoro-3-(trifluoromethyl)phenyl]-4-oxobut-2-enamide (**ASDO2**) was made according to the general procedure reported for **ASDO1**. ^{1}H NMR (500 MHz, Chloroform-*d*) δ 10.29 (s, 1H), 8.58 (d, *J* = 4.6 Hz, 1H), 8.25 – 8.18 (m, 2H), 7.89 (d, J = 15 Hz, 1H), 7.82 (d, J = 10 Hz, 2H), 7.57 (d, J = 10 Hz, 2H), 7.33 (d, J = 15 Hz, 1H), 7.30 – 7.25 (m, 2H), 6.03 (s, 2H), 5.05 (hept, *J* = 6.5 Hz, 1H), 1.48 (d, *J* = 6.5 Hz, 6H). ^{13}C NMR (126 MHz, $CDCl_3$) δ 190.8, 156.9, 153.7, 150.4, 146.9, 143.7, 143.5, 139.3, 138.0, 134.7, 131.6, 129.0, 128.9, 128.5, 120.6, 120.6, 120.0, 117.7, 117.5, 100.2, 39.4, 20.8. LCMS-LCQ: 4 mins, 5-95% MeCN, Rt = 0.62 mins, > 99% purity; $[M+H]^+$ calculated for $C_{25}H_{20}F_4N_6O_2$ 513.16; found 513.19. HRMS (ESI): $[M+H]^+$ calculated for $C_{25}H_{20}F_4N_6O_2$ 513.1583, found 513.1659.

(2E)-N-{4-[4-Amino-1-(propan-2-yl)-1H-pyrazolo[3,4-d]pyrimidin-3-yl]phenyl}-4-[4-chloro-3-(trifluoromethyl)phenyl]-4-oxobut-2-enamide (**ASDO3**) was made according to the general procedure reported for **ASDO1**. ^{1}H NMR (500 MHz, Chloroform-*d*) δ 10.40 (s, 1H), 9.66 (s, 1H), 8.28 (s, 1H), 8.21 (s, 1H), 8.09 (d, *J* = 8.3 Hz, 1H), 7.93 (s, 1H), 7.90 – 7.87 (m, 3H), 7.62 (d, *J* = 8.4 Hz, 1H), 7.55 – 7.52 (m, 2H), 7.34 (d, *J* = 14.9 Hz, 1H), 6.86 (s, 2H), 5.10 (hept, *J* = 6.8 Hz, 1H), 1.52 (d, *J* = 6.7 Hz, 6H). ^{13}C NMR (126 MHz, $CDCl_3$) δ 188.2, 152.2, 150.8, 146.9, 143.9, 143.8, 137.3, 136.4, 135.5, 131.9, 130.6, 130.1, 130.1, 129.5, 129.5, 126.8, 125.6, 125.6, 124.5, 97.6, 34.5, 21.8. LCMS-LCQ: 4 mins, 5-95% MeCN, Rt = 0.65 mins, > 99% purity; $[M+H]^+$ calculated for $C_{25}H_{20}ClF_3N_6O_2$ 529.12; found 529.15. HRMS (ESI): $[M+H]^+$ calculated for $C_{25}H_{20}ClF_3N_6O_2$ 529.1288, found 529.1359.

(2E)-N-{4-[4-amino-1-(propan-2-yl)-1H-pyrazolo[3,4-d]pyrimidin-3-yl]naphthalen-1-yl}-4-oxo-4-[3-(trifluoromethyl)phenyl]but-2-enamide (**ASDO4**) was made according to the general procedure reported for **ASDO1**. ^{1}H NMR (500 MHz, Chloroform-*d*) ^{1}H NMR (500 MHz, Chloroform-*d*) δ 9.55 (s, 1H), 8.39 (s, 1H), 8.34 (s, 2H), 8.27 (s, 1H), 8.18 (d, *J* = 14.7 Hz, 1H), 8.01 (d, *J* = 8.7 Hz, 1H), 7.91 (d, *J* = 7.9 Hz, 1H), 7.72 (d, *J* = 7.6 Hz, 1H), 7.64 (t, *J* = 8.0 Hz, 1H), 7.58 (t, *J* = 7.6 Hz, 1H), 7.45 (d, *J* = 14.7 Hz, 1H), 5.49 (s, 2H), 5.28 (hept, *J* = 6.5 Hz, 1H), 1.67 (d, *J* = 6.8 Hz, 6H). ^{13}C NMR (126 MHz, $CDCl_3$) δ 188.09, 176.93, 164.36, 157.07, 154.49, 137.26, 136.07, 133.89, 133.13, 131.95, 131.91, 130.27, 129.98, 129.74, 129.62, 128.36, 127.67, 127.61, 127.55, 127.32, 126.59, 125.68, 125.65, 125.62, 120.25, 100.23, 49.31, 22.05. LCMS-LCQ: 4 mins, 5-95% MeCN, Rt = 0.61 mins, > 99% purity; $[M+H]^+$ calculated for $C_{29}H_{23}F_3N_6O_2$ 545.18; found 545.25. HRMS (ESI): $[M+H]^+$ calculated for $C_{29}H_{23}F_3N_6O_2$ 545.1835, found 545.2167.

(2E)-N-{4-[4-Amino-1-(propan-2-yl)-1H-pyrazolo[3,4-d]pyrimidin-3-yl]-3-methylphenyl}-4-[4-fluoro-3-(trifluoromethyl)phenyl]-4-oxobut-2-enamide (**ASDO6**) was made according to the general procedure reported for **ASDO1**. ^{1}H NMR (500 MHz, Chloroform-*d*) δ 8.97 (s, 1H), 8.37 (s, 1H), 8.35 (d, 1H), 8.32 – 8.26 (m, 1H), 8.24 (d, *J* = 8.2 Hz, 1H), 8.09 (d, *J* = 14.8 Hz, 1H), 7.62 – 7.57 (m, 2H), 7.38 (t, *J* = 9.1 Hz, 1H), 7.29 (s, 1H), 5.75 (s, 2H), 5.19 (hept, *J* = 6.7 Hz, 1H), 2.43 (s, 3H), 1.61 (d, *J* = 6.8 Hz, 6H). ^{13}C NMR (126 MHz, $CDCl_3$) δ 186.6, 161.6, 157.2, 154.5, 153.3, 143.4, 136.3, 135.9, 134.8, 134.7, 133.2,

133.1, 130.8, 130.7, 129.7, 128.6, 128.5, 126.9, 123.2, 118.0, 117.8, 98.4, 77.3, 49.1, 22.0, 17.9. LCMS-LCQ: 4 mins, 5-95% MeCN, Rt = 2.89 mins, > 95% purity; $[M+H]^+$ calculated for $C_{26}H_{22}F_4N_6O_2$ 527.17; found 527.21. HRMS (ESI): $[M+H]^+$ calculated for $C_{26}H_{22}F_4N_6O_2$ 527.1740, found 527.2500.

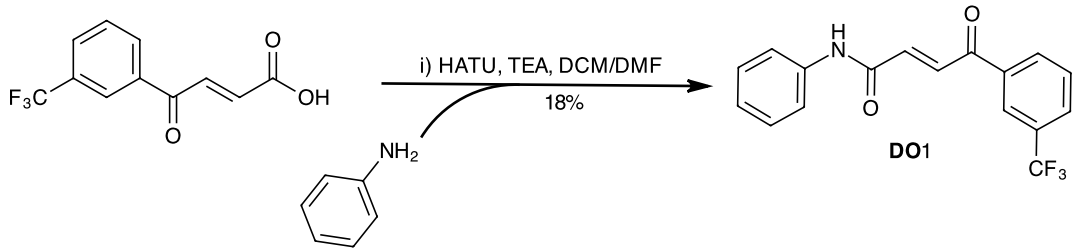

(*E*)-4-Anilino-1-[*m*-(trifluoromethyl)phenyl]-2-butene-1,4-dione (**DO1**) was made by dissolving (E)-4-oxo-4-[3-(trifluoromethyl)phenyl]but-2-enoic acid (80 mg, 0.33 mmol, 1.5 eq.) in DCM (2mL) and DMF (200uL) in an oven dried, Ar (g) cooled 20 mL scintillation vial with septum top. TEA (61 uL, 0.44 mmol, 2 eq.) and HATU (133 mg, 0.35 mmol, 1.6 eq.) were then added and the mixture was allowed to stir at RT for 15 min. Next, the solution was chilled to 0 °C before the drop-wise addition of aniline (20 uL, 0.22 mmol, 1 eq.). After 10 min., the reaction was warmed to RT, stirred for an hour and then warmed to 40 °C. After mixing for 1 h at 40 °C, the reaction was cooled and then quenched with 25 mL $NAHCO_3$. This mixture was extracted 2X with DCM, dried with $MgSO_4$ and concentrated *in vacuo*. Purification was achieved by silica chromatography using a hexanes/ethyl acetate system (ethyl acetate gradient increased over time from 0 – 100%). Concentration of the fractions yielded 12.9 mg (18%) of **DO1**.^{1}H NMR (400 MHz, DMSO-d_6) δ 10.63 (s, 1H), 8.38 (d, *J* = 7.9 Hz, 1H), 8.31 (s, 1H), 8.12 – 8.06 (m, 1H), 7.95 (d, *J* = 15.2 Hz, 1H), 7.85 (t, *J* = 7.8 Hz, 1H), 7.73 (dd, *J* = 8.6, 1.0 Hz, 2H), 7.41 – 7.34 (m, 2H), 7.26 (d, *J* = 15.2 Hz, 1H), 7.16 – 7.09 (m, 1H). ^{13}C NMR (100 MHz, DMSO) δ 189.2, 162.1, 139.1, 137.8, 137.7, 133.2, 133.0, 130.8, 130.5, 130.4, 130.3, 130.0, 129.4, 125.4, 125.4, 124.6, 119.9.

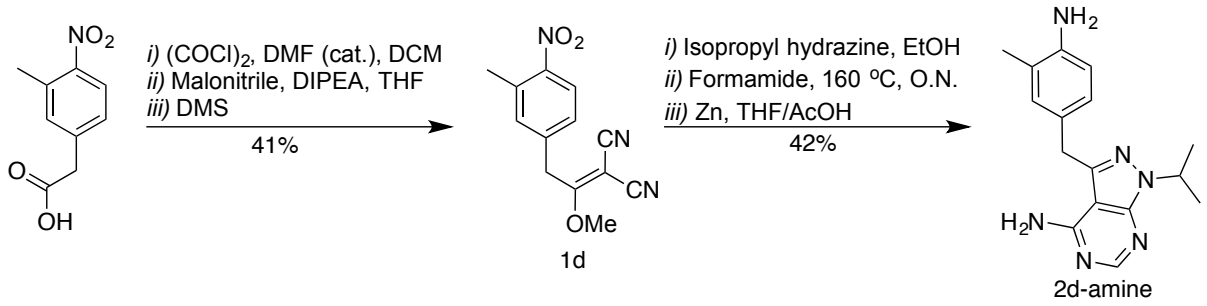

2-[1-methoxy-2-(3-methyl-4-nitrophenyl)ethylidene]propanedinitrile (**1d**) was made according to the general procedure reported for **1a**. ^{1}H NMR (500 MHz, Chloroform-*d*) δ 7.96 (d, 1H), 7.26 (m, 2H), 3.73 (s, 3H), 3.68 (s, 2H), 2.61 (s, 3H).

3-[(4-amino-3-methylphenyl)methyl]-1-(propan-2-yl)-1H-pyrazolo[3,4-d]pyrimidin-4-amine (**2d-amine**) was made according to the general procedure reported for **2a** followed by reduction with Zn dust as reported in the first Zn-reduction step of the general procedure for the coupling of 3-benzoylacrylic acids

with 3-phenyl pyrazolopyrimidines. The amine was purified by silica chromatography using a DCM/ethyl acetate solvent system (ethyl acetate gradient increased over time from 0 – 50%). This coupling partner is hindered, and thus we needed to reduce the nitro substituted precursor and obtain a very pure sample of the amine to carry on through to the next coupling step. ^{1}H NMR (500 MHz, Chloroform-*d*) δ 8.11 (s, 1H), 6.77 (s, 1H), 6.75 (d, *J* = 7.9 Hz, 1H), 6.52 (d, *J* = 8.1 Hz, 1H), 5.47 (s, 2H), 4.97 (hept, *J* = 6.7 Hz, 1H), 4.06 (s, 2H), 3.55 (s, 2H), 2.00 (s, 3H), 1.46 (d, *J* = 6.7 Hz, 6H). ^{13}C NMR (126 MHz, $CDCl_3$) δ 157.0, 153.8, 152.7, 144.2, 144.0, 132.0, 130.3, 126.7, 123.1, 115.4, 99.9, 48.4, 34.2, 21.8, 17.3.

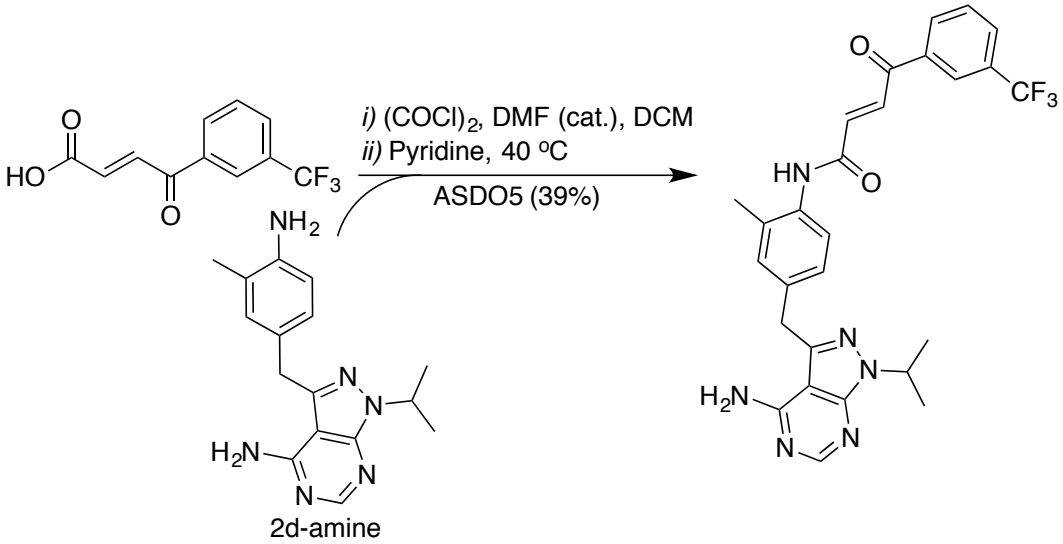

(2E)-N-(4-{[4-amino-1-(propan-2-yl)-1H-pyrazolo[3,4-d]pyrimidin-3-yl]methyl}-2-methylphenyl)-4-oxo-4-[3-(trifluoromethyl)phenyl]but-2-enamide (**ASDO5)** was made according to the general procedure reported for **ASDO1** starting from the amine. ^{1}H NMR (500 MHz, Chloroform-*d*) δ 9.33 (s, 1H), 8.32 (s, 1H), 8.25 (d, *J* = 8.0 Hz, 1H), 8.19 (s, 1H), 8.12 – 8.06 (m, 2H), 7.90 (d, *J* = 7.8 Hz, 1H), 7.75 (s, 1H), 7.69 (t, *J* = 7.9 Hz, 1H), 7.32 (d, *J* = 14.9 Hz, 1H), 7.14 (d, *J* = 8.4 Hz, 1H), 5.58 (s, 2H), 5.16 (hept, *J* = 6.8 Hz, 1H), 4.33 (s, 2H), 2.34 (s, 3H), 1.63 (d, *J* = 6.6 Hz, 6H). ^{13}C NMR (126 MHz, $CDCl_3$) δ 188.2, 176.4, 173.3, 167.0, 165.8, 152.3, 150.0, 146.9, 143.9, 137.3, 136.5, 135.5, 131.9, 130.7, 130.1, 129.5, 126.8, 125.6, 124.5, 97.6, 50.2, 34.5, 21.8, 18.2. LCMS-LCQ: 7 mins, 5-95% MeCN, Rt = 3.09 mins, > 99% purity; $[M+H]^+$ calculated for $C_{27}H_{25}F_3N_6O_2$ 523.1990; found 523.21. HRMS (ESI): $[M+H]^+$ calculated for $C_{27}H_{25}F_3N_6O_2$ 523.1990, found 523.4167.

^{1}H and ^{13}C NMR Spectra and LCMS Analysis

ASDO1 ^{1}H NMR (400 MHz, DMSO-*d6*)

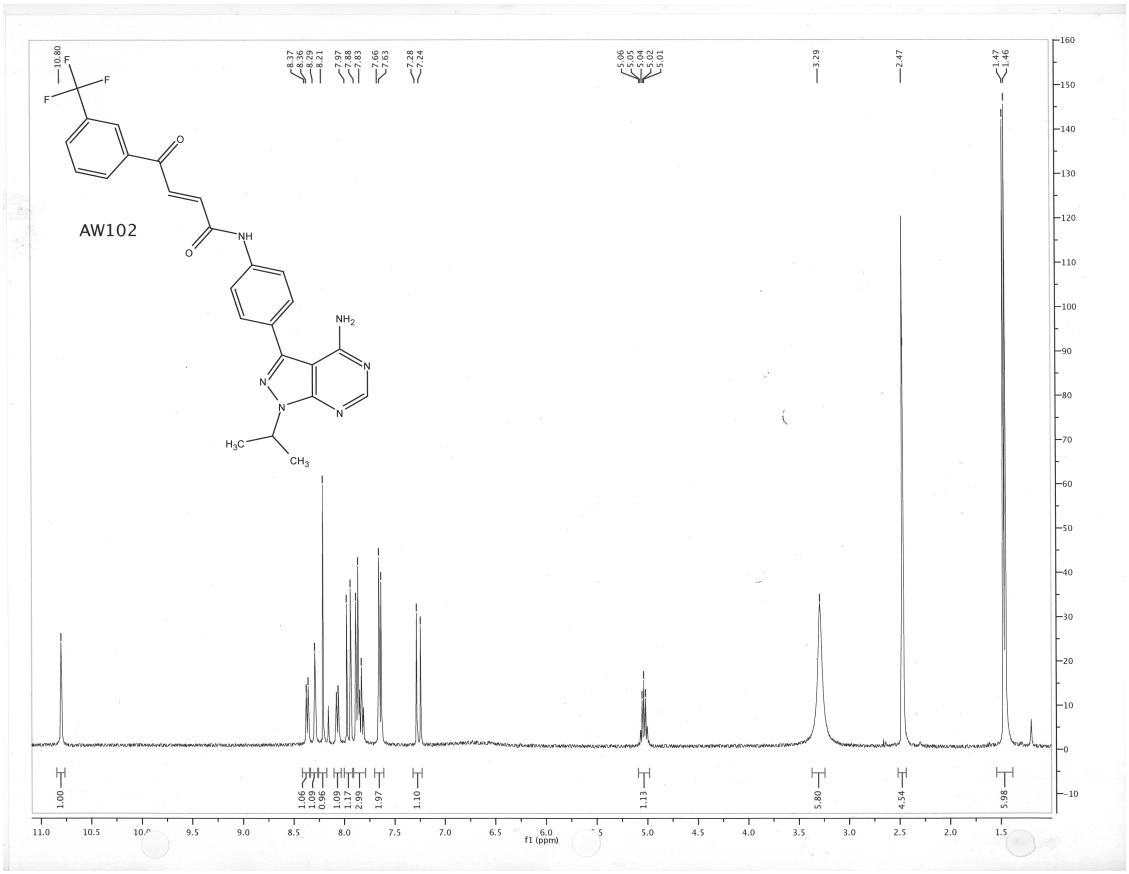

ASDO1 ^{13}C NMR (126 MHz, $CDCl_3$): It should be noted that we did not detect C-F heteronuclear coupling due to CF_3 in the ^{13}C NMR mainly due to overlapping peaks.

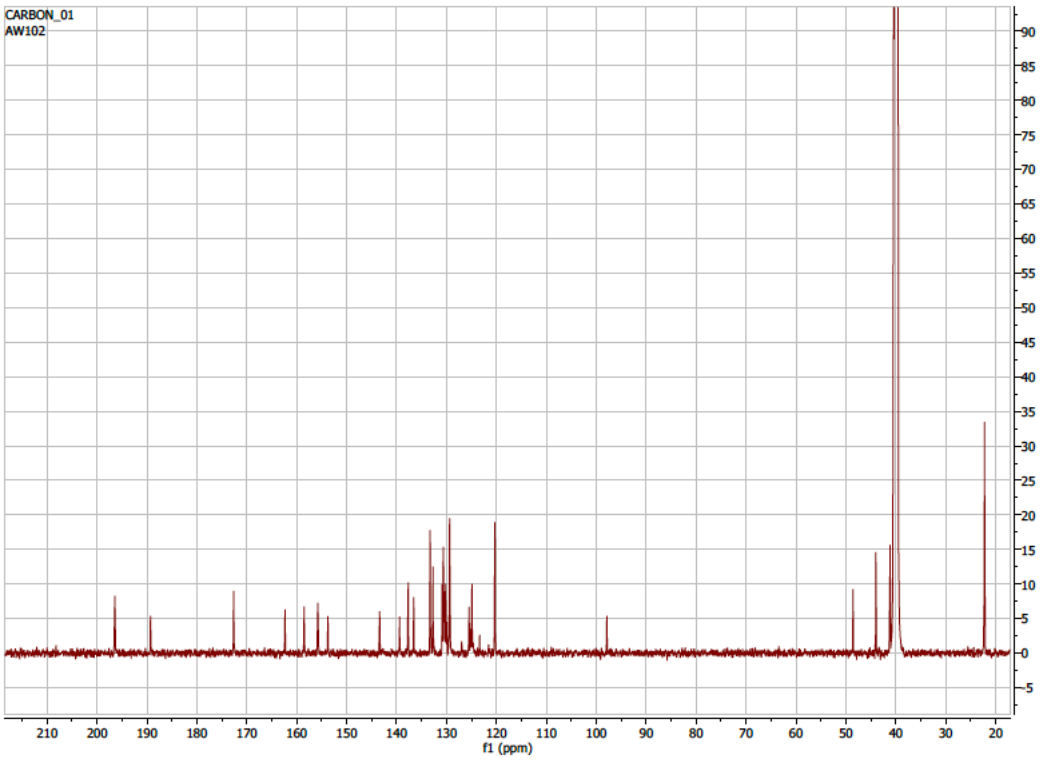

ASDO1 LCMS

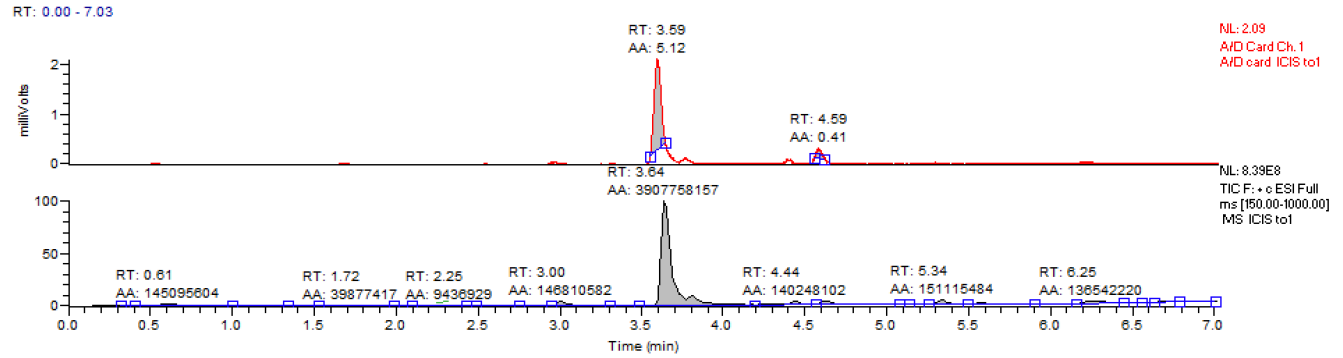

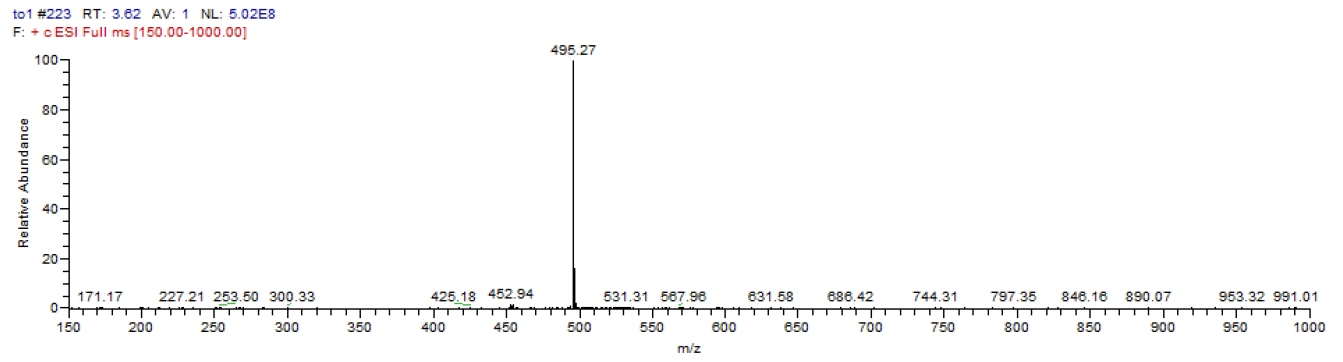

ASDO2 ^{1}H NMR (500 MHz, 1:1 Chloroform-*d*:DMSO-*d6*)

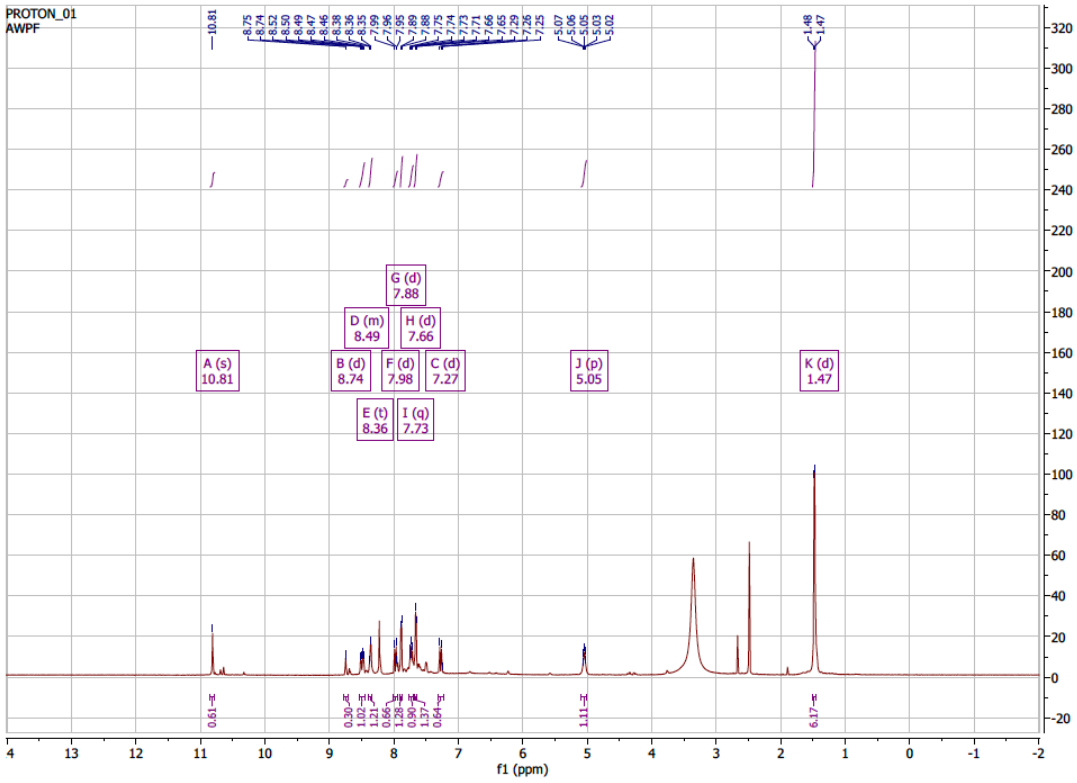

ASDO2 ^{13}C NMR (126 MHz, 1:1 $CDCl_3$:DMSO-*d6*): It should be noted that we did not detect C-F heteronuclear coupling due to CF_3 in the ^{13}C NMR mainly due to overlapping peaks.

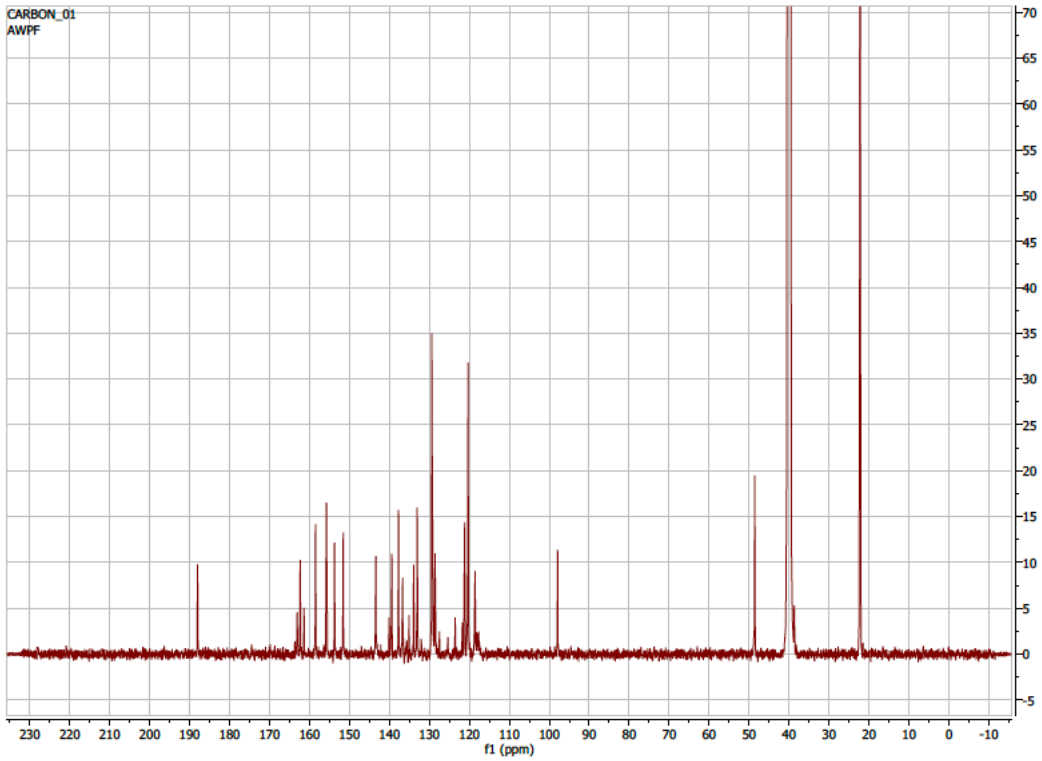

ASDO2 LCMS

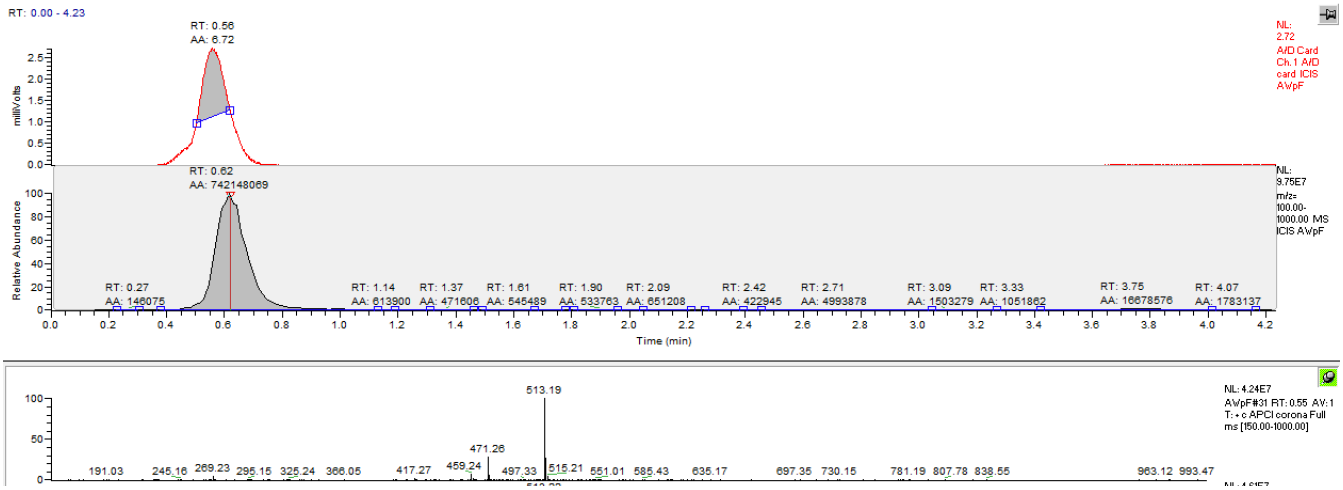

ASDO6 ^{1}H NMR (500 MHz, Chloroform-*d*)

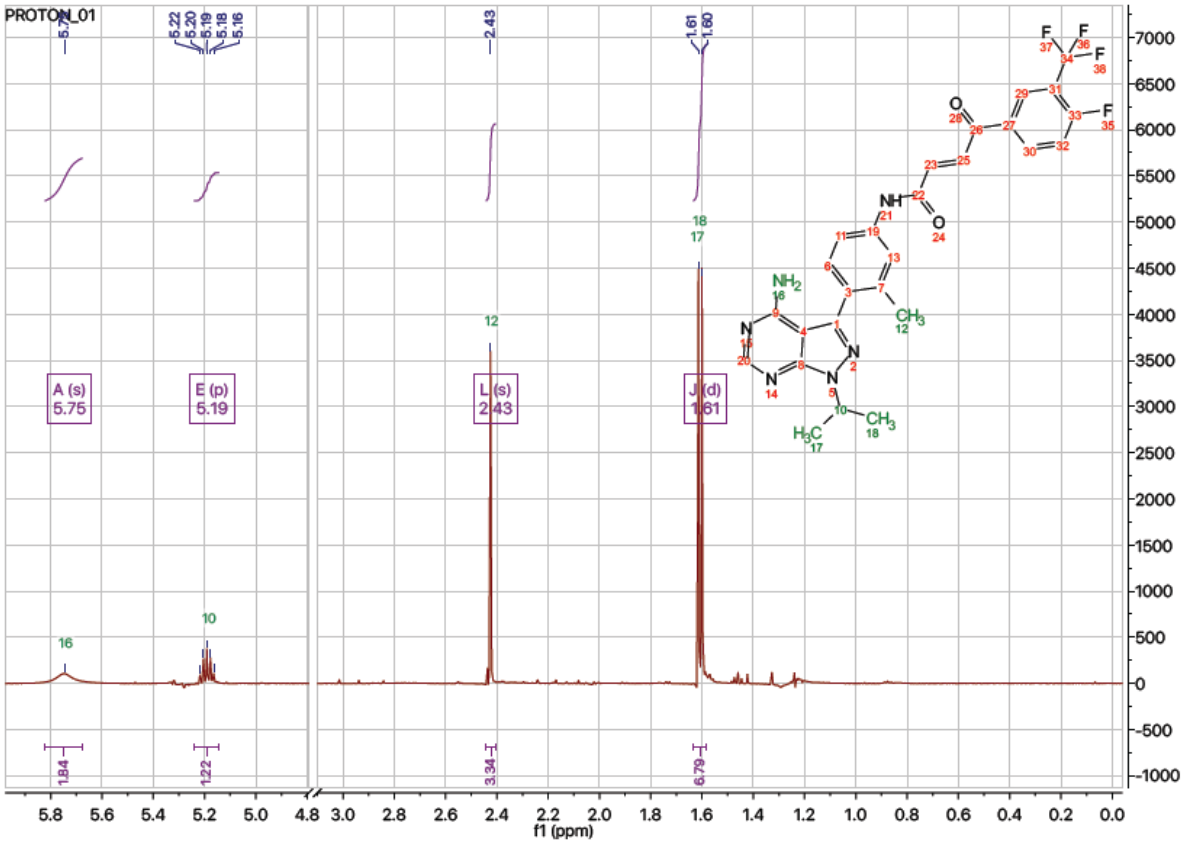

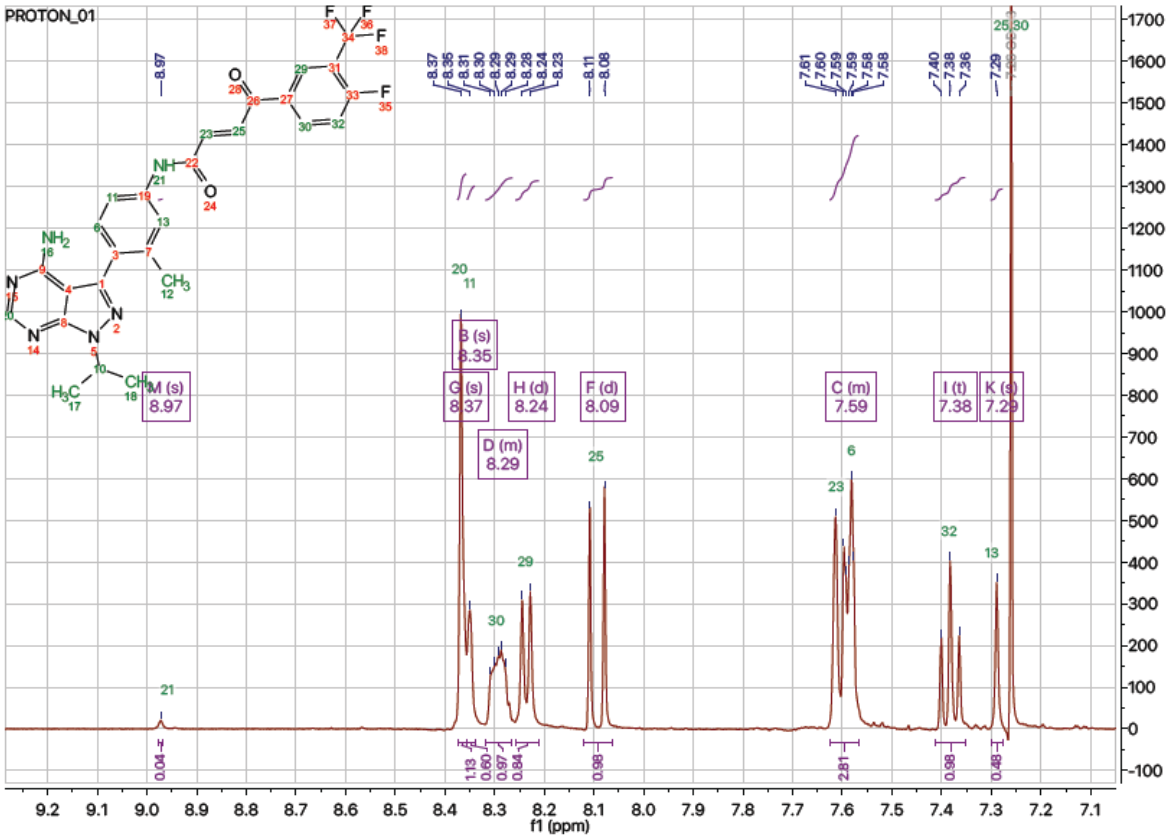

ASDO6 ^{13}C NMR (126 MHz, $CDCl_3$): It should be noted that we did not detect C-F heteronuclear coupling due to CF_3 in the ^{13}C NMR mainly due to overlapping peaks.

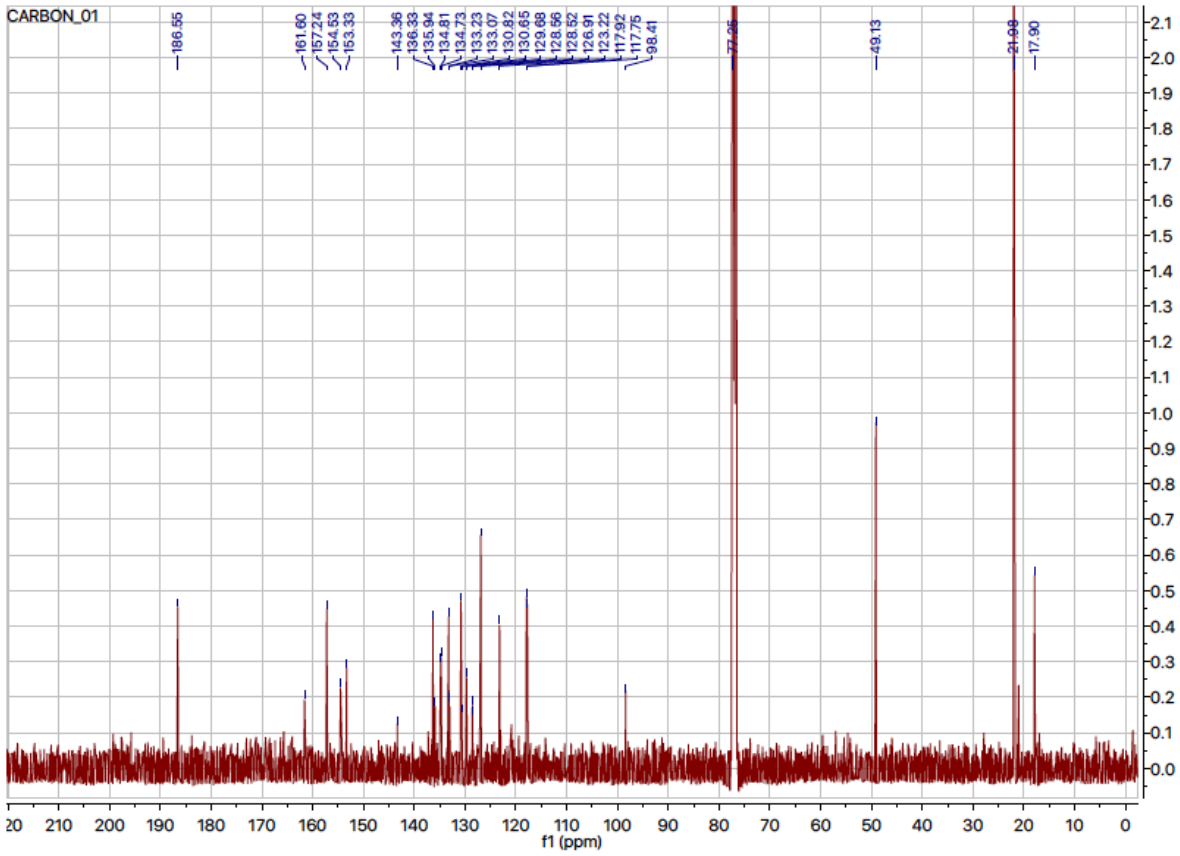

ASDO6 LCMS

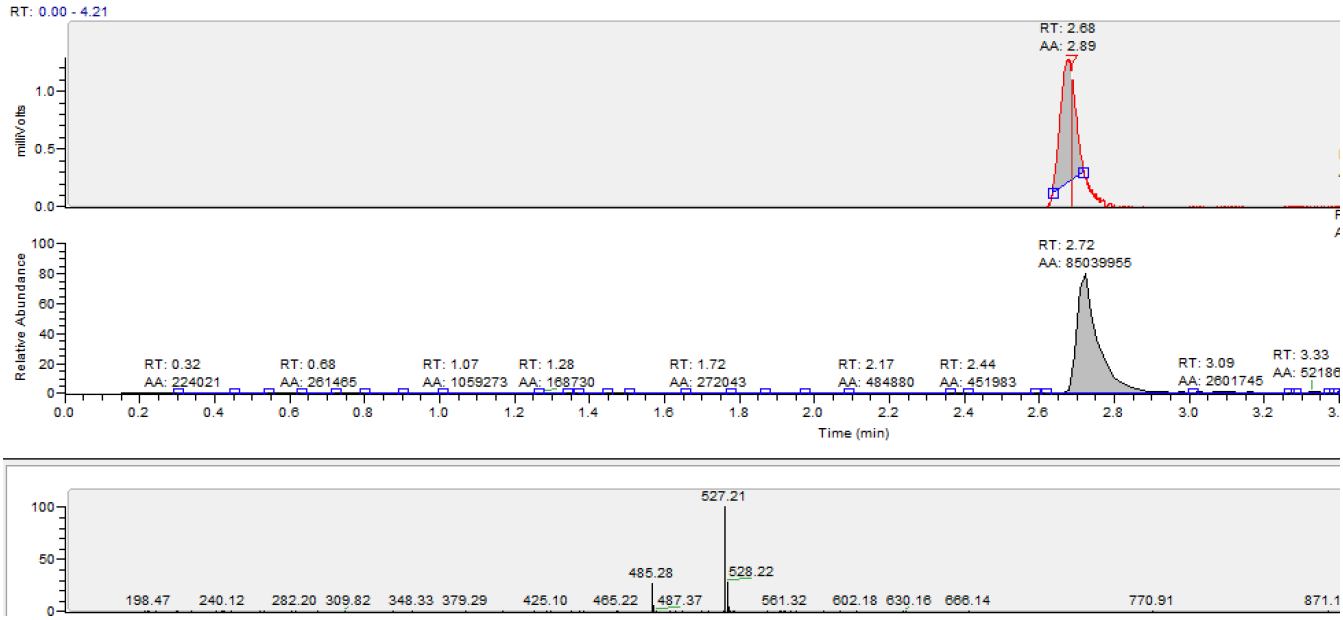

References

[1] Garske, A. L., Peters, U., Cortesi, A. T., Perez, J. L., and Shokat, K. M. (2011) Chemical genetic strategy for targeting protein kinases based on covalent complementarity, *Proc Natl Acad Sci U S A 108*, 15046-15052.

[2] Tolstoluzhsky, N., Nikolaienko, P., Gorobets, N., Van der Eycken, E. V., and Kolos, N. (2013) Efficient Synthesis of Uracil-Derived Hexa- and Tetrahydropyrido[2,3-d]pyrimidines, *European Journal of Organic Chemistry 2013*, 5364-5369.